R-02-24

Site-scale groundwater flow modelling of Aberg and upscaling of conductivity

Douglas Walker

Watermark Group, Inc

Björn Gylling

Kemakta Konsult AB

April 2002

SKB

Site-scale groundwater flow modelling of Aberg and upscaling of conductivity

Douglas Walker
Watermark Group, Inc

Björn Gylling
Kemakta Konsult AB

April 2002

Abstract

A recent performance assessment study of spent nuclear fuel disposal in Sweden, Safety Report 1997 (SR 97) included modelling of flow and transport in fractured host rocks. Hydraulic conductivity measurements in this system exhibit a strong scale dependence that needed to be addressed when determining the mean and variogram of the hydraulic conductivity for finite-difference blocks and when nesting site-scale models within regional scale models. This study applies four upscaling approaches to the groundwater flow models of Aberg, one of the hypothetical SR 97 repositories. The approaches are: 1) as in SR 97, empirically upscaling the mean conductivity via the observed scale dependence of measurements, and adjusting the covariance via numerical regularisation; 2) empirically upscaling as in SR 97, but considering fracture zones as two-dimensional features; 3) adapting the effective conductivity of stochastic continuum mechanics to upscale the mean, and geostatistical regularisation for variogram; and 4) the analytical approach of /Indelman and Dagan, 1993a/. These four approaches are evaluated for their effects on simple measures of repository performance including the canister flux, the advective travel time from representative canister locations to the ground surface, and the F-quotient. A set of sensitivity analyses suggest that the results of the SR 97 Aberg Base Case are insensitive to minor computational changes and to the changes in the properties of minor fracture zones. The comparison of alternative approaches to upscaling indicates that, for the methods examined in this study, the greatest consistency of boundary flows between the regional and site-scale models was achieved when using the scale dependence of hydraulic conductivity observed at Äspö for the rock domains, the hydraulic conductivities of the large-scale interference tests for the conductor domain, and a numerical regularisation based on Moye's formula for the variogram. The assumption that the fracture zones of the SCD behave as two-dimensional media results in the greatest change to the median travel time, and improves agreement between the boundary flows of the regional and site-scale models. The improved flow balance suggests that domains that act as two- or three-dimensional features should use upscaling algorithms tailored to their dimensionality. The comparison of alternative approaches to upscaling indicates that, for the methods examined in this study, the uncertainty implied by choice of upscaling method has a relatively small impact on median performance measures. The greatest impacts of upscaling uncertainty appear to be on the variances and earliest arrival times of particles released from representative canister positions. However, the impacts of upscaling uncertainty appear to be small relative to the impacts of other uncertainties in the performance assessment of a repository for nuclear waste disposal.

Sammanfattning

I en nyligen utförd säkerhetsanalysstudie av djupförvaring av använt kärnbränsle i Sverige, Säkerhetsrapport 1997 (SR 97), modellerades grundvattenflöde och transport i sprickigt berg. Mätningar av hydraulisk konduktivitet i detta medium påvisar ett starkt skalberoende vilket man behövde ta hänsyn till när medelvärde och variogram av hydraulisk konduktivitet utvärderades för finita differensblock och när man nästlade platsskalemodeller i regionala modeller. I den föreliggande studien appliceras fyra ansatser för uppskalning på grundvattenmodeller av Aberg, ett av de hypotetiska djupförvaren i SR 97. Ansatserna är: 1) som i SR 97, dvs empirisk uppskalning av medelvärde för konduktivitet med hjälp av ett från mätningar observerat skalberoende samt justering av kovariansen med hjälp av numerisk regularisering; 2) empirisk uppskalning som i SR 97, men här behandlas sprickzoner som tvådimensionella enheter; 3) användande av effektivvärde för konduktivitet erhållen genom en stokastisk kontinuum teknik för att skala upp medelvärdet samt genom att använda geostatistisk regularisering för att erhålla variogram; och 4) en analytisk metod föreslagen av /Indelman och Dagan, 1993a/. Dessa fyra ansatser utvärderas med avseende på deras effekt på förenklade mått av förvarsfunktionen. Måtten inkluderar specifikt flöde vid kapselpositioner, advektiv gångtid från representativa kapselpositioner upp till markytan samt F-faktorn. Utförda känslighetsanalyser påvisar att resultaten för basfallet av Aberg i SR 97 är okänsligt för mindre ändringar i datorberäkningarna och för ändringar i egenskaperna för mindre sprickzoner. Jämförelsen av de alternativa ansatserna för uppskalning som undersökts i denna studie visar på att den bästa överensstämmelsen för vattenflöde över ränderna mellan regionalmodell och platsskalemodell erhölls för ansats 2 enligt ovan. I denna ansats används det för Aberg observerade skalberoendet inom bergmassedomäner, de värden som uppmätts i storskaliga pumptest används inom sprickzonsdomäner och numerisk regularisering baserad på Moyes ekvation används för att erhålla variogram. Antagandet att sprickzoner inom SCD agerar som tvådimensionella media resulterar i den största förändringen av medelvärdet för gångtider och förbättrar överensstämmelsen av randflöden mellan regional- och platsskalemodell. Den förbättrade flödesbalansen indikerar att domäner som fungerar som två- eller tredimensionella enheter bör uppskalas med algoritmer i enlighet med enheternas dimensionalitet. Jämförelsen av de alternativa ansatserna för uppskalning som undersökts i denna studie påvisar att osäkerheten relaterad till val av uppskalningsmetod har relativt sett en liten effekt på medianvärdena för måtten på förvarsfunktionen. Den största påverkan av denna osäkerhet relaterad till uppskalningsmetod erhålls tillsynes på varianserna och fraktionen med de kortaste gångtiderna av de partiklar som släpps från representativa kapselpositioner. Effekten av osäkerheten i uppskalningsmetod verkar emellertid vara liten i förhållande till andra osäkerheter inom en säkerhetsanalys av ett djupförvar för använt kärnbränsle.

Contents

1   Introduction

The Safety Report 1997 (SR 97), conducted by the Swedish Nuclear Fuel and Waste Management Company (SKB), presents a comprehensive performance assessment of the long-term safety of three hypothetical repositories for spent nuclear fuel. The performance assessment of each repository includes geosphere modelling to examine the possible transport of radionuclides from the emplaced waste packages through the host rock to the accessible environment. Ideally, the model parameters such as hydraulic conductivity should be based on site-specific measurements to lend credibility and realism to the results. However, using small-scale measurements of hydraulic conductivity directly in large-scale numerical models can be problematic, since hydraulic conductivity can be a scale-dependent parameter. In hydrogeologic modelling, the adaptation of small-scale measurements for use in larger-scale models is referred to as upscaling. Although several methods for upscaling have been proposed, upscaling of hydraulic conductivity is not well understood in the case of fractured media.

Hydrogeologic modelling in SR 97 idealizes the host rocks as two hydrogeologic units: the relatively intact bedrock of low conductivity, and the relatively conductive fracture zones. The hydraulic conductivities of these units were represented as spatially correlated, random variables, whose distributions were inferred from upscaled measured values of hydraulic conductivity. SR 97 used a nested modelling approach, with a deterministic regional model providing boundary conditions for the stochastic site scale model. This use of separate domains, nested modelling, and multiple test scales in SR 97 compounds the difficulty of upscaling the measured hydraulic conductivities to numerical block values. SR 97 addressed the upscaling of mean hydraulic conductivity using the observed scale dependency of hydraulic tests and a numerical regularisation to determine the covariance of block conductivity. Variant cases briefly evaluated this approach to upscaling for self-consistency and found it to be acceptable, but alternative methods for upscaling were not tested. Each of these alternative methods might result in different conclusions regarding groundwater flow, injecting uncertainty into the performance assessment.

The objective of this study is to evaluate uncertainties regarding the upscaling of hydraulic conductivity for their impact on groundwater flow modelling for performance assessments for disposal of nuclear waste. This study applies four upscaling approaches to the groundwater flow models of one of the hypothetical SR 97 repositories: 1) as in SR 97, empirically upscaling the mean conductivity via the observed scale dependence of measurements, and adjusting the covariance via numerical regularisation; 2) empirically upscaling as in SR 97, but considering fracture zones as two-dimensional features; 3) adapting the effective conductivity of stochastic continuum mechanics to upscale the mean, and geostatistical regularisation for covariance; and 4) the analytical approach of /Indelman and Dagan, 1993b/. These four approaches will be evaluated for the effects on simple measures of repository performance and for the consistency of boundary flows between the regional and site-scale models. The report summarises the

site conditions, the modelling strategy and the model application. This is followed by a description of each upscaling method, and a comparison of each method's results for the SR 97 base case.

2   Background

This section presents the SR 97 approach to hydrogeologic modelling, including the characterisation, inference, and flow modelling at the site of interest. It summarises a series of documents produced as part of SR 97, including the site characterisation studies /Rhén et al, 1997/, inference of model parameters /Walker et al, 1997/, groundwater flow modelling /Walker and Gylling, 1998; Walker et al, 2001/, uncertainty analysis /Selroos et al, 2002/, and performance assessment /SKB, 1999/.

2.1   Modelling approach

This study, like SR 97, analyses groundwater flow and advective travel times in fractured crystalline host rocks via the stochastic continuum (SC) modelling approach. This approach assumes that, over some representative volume, the heterogeneity of the media may be represented as an equivalent homogeneous porous medium with groundwater flow governed by Darcy's law. The hydraulic conductivity of the equivalent system is treated as a random spatial distribution of hydraulic conductivities that represent spatially averaged fracture properties. Monte Carlo realisations of the hydraulic conductivities are used as input to numerical groundwater flow models which provide groundwater velocities, flow paths, and advective travel times from the hypothetical waste canisters /Neuman, 1988/.

The numerical modelling of SR 97 idealizes the host rocks as two hydrogeologic units: the relatively intact bedrock of low conductivity, referred to as the Rock Domain, and the relatively conductive fracture zones, referred to as the Conductor Domain (RD and CD, respectively). On the site scale, a detailed structural map provides the site-scale conductor domain (SCD) and the site-scale rock domain (SRD); the regional-scale counterparts are denoted RCD and RRD. Conductors are identified based on increased fracturing, increased hydraulic conductivity, or both, and range from a few meters to over 100 meters in width. The site-scale model requires a domain of adequate grid density to represent the deterministic SCD, yet extensive enough to include the regional-flow patterns. This study thus adopts a nested modelling approach similar to that of /Ward et al, 1987/, with the stochastic, site-scale model taking its boundary conditions from a deterministic, regional-scale model. This nesting approach leads to a relatively dense site-scale model that incorporates regional flow by assigning the regional-model heads to the site-scale domain boundaries. The boundary heads are taken from a steady-state, deterministic regional model whose hydraulic conductivities are manually calibrated to reproduce the observed gradients, discharge patterns, and approximate runoff rates. The head values of the regional model are transferred to the denser site-scale model grid using first-order interpolation between the widely spaced regional model nodes. Flow balances between the regional- and site-scale models provide a check on the consistency of the upscaling of hydraulic conductivity.

This study uses HYDRASTAR, a SC model developed to support the SKB 91 safety analysis project /SKB, 1992/. HYDRASTAR simulates log-normally distributed, heterogeneous hydraulic conductivity fields as a continuous, spatially correlated stochastic process (i.e., a regionalized variable). Geostatistical simulation is used to create hydraulic-conductivity fields, using stepwise changes in the mean of $\log_{10}$ hydraulic conductivity to represent the Conductor Domain and decrease of conductivity with depth. A node centred finite-difference numerical approach solves the governing equations for 3-D groundwater flow within the simulated conductivity fields, followed by advective particle tracking to determine the advective transport path from each canister position. /Gylling and Eriksson, 2001/ summarize the features and testing of HYDRASTAR.

Note that HYDRASTAR is restricted to lognormally distributed hydraulic conductivity fields, generated by its own Turning Bands algorithm, and cannot read in an externally-generated hydraulic conductivity field. As is discussed further in Section 3, this limits the choice of upscaling approaches that can be considered in this study.

This study examines upscaling within the Base Case scenario of SR 97, which is the set of reasonable assumptions for site conditions and parameters, pragmatically taken to be the plausible models of the physical processes generally believed to be involved at the site. The Base Case parameter values are taken as the best estimates inferred from the available data /Andersson et al, 1998/. The Base Case uses steady-state, freshwater conditions, with constant-head boundaries and unconditionally simulated, multivariate lognormal hydraulic conductivity fields.

2.2   Performance measures

Repository performance is ultimately judged by the probable radiation dose to humans, but dose calculations also include the effects of waste-package failure, the human exposure model, etc. Because these additional process models may obscure the impacts of variations in hydrogeologic models and parameters, this study examines the statistics of simple geosphere performance measures rather than the dose. The first of these measures is the canister flux, calculated as the flow of groundwater per unit area (Darcian velocity) at each representative canister position. Other intersite comparison studies have used Darcy velocity as a performance measure, calculated for simplified representative flow paths /e.g., Dverstorp et al, 1996/ or at repository level /KBS, 1983/. However, Darcy velocity alone is an inadequate measure because it ignores travel-path length and complexity, requiring this study also to examine other performance measures. One of these is the advective travel time, t_w, from representative canister locations to the ground surface. Because HYDRASTAR is limited to a homogeneous flow porosity, ε_f, the reported travel times are directly proportional to the assumed value of flow porosity. The last performance measure is the F-quotient [years/m], defined for media with homogeneous flow wetted surface and porosity, as:

$$F \quad = \quad \frac{d_w \, a_r}{q_w} \quad = \quad t_w \, a_w \qquad\qquad (2\text{-}1)$$

where d_w is the advective travel distance [m]; q_w is the Darcy velocity $= v \, \varepsilon_f$ [m/year]; a_r is the specific flow-wetted surface per rock volume [m^{-1}]; a_w is the specific flow-wetted surface per volume of water [m^{-1}]; and t_w is the advective travel time [year]. The F-quotient is useful in evaluating repository performance since the transit time may depend on both the advective velocity and on the surface area available for rock interaction /SKI, 1997/. Note that if porosity and the specific flow-wetted surface are homogeneous, the F-quotient is simply a rescaled travel time. Also note that the F-quotient, like the advective travel time, is obtained through integration along pathlines /Andersson et al, 1998/.

The study compares two characteristics of the performance measures. The first characteristic is the expected model behaviour, which can reveal possible systematic bias (i.e., do the models provide mean predictions consistent with each other and with observed patterns?). The second characteristic to compare is the variability of the performance measures to assess whether differences exist with respect to the range or spread of the predicted measures. The comparisons are based on statistics of travel time, canister flux and F-quotient averaged over all canisters, which are sorted into various sets. The statistics collected include the sample arithmetic mean and variance (as estimators of the true mean and true variance); the sample median; and the sample 5th and 95th percentiles. Since the performance measures are expected to have a wide range and the distributions positively skewed, all statistics are calculated for the common logarithm of the performance measures.

2.3   Site description

This study examines upscaling as applied to Aberg, one of the SR 97 hypothetical repositories, which adopts its input parameters from the Äspö site, an area previously investigated by SKB. Äspö itself is an island just off the south-eastern Swedish coast in the Baltic Sea (Figure 2-1). The geology and hydrogeology of the Äspö site have been studied in detail, beginning in 1986 /Rhén et al, 1997; Walker et al, 1997/. Fractured granites dominate the Äspö regional geology, with thin overlying soils and bouldery till, fluvial sand, gravel, and peatlands. Remote sensing, and geophysical and borehole studies offsite have revealed a number of regional lineaments that have been interpreted as steeply-dipping fracture zones. Site-characterisation studies have included geophysical surveys (aerial, surface, and subsurface), subsurface drilling, hydraulic tests (double-packer, pumping, interference, spinner), and tracer tests. Hydraulic tests have been performed at multiple scales in all boreholes, including exhaustive coverage of the cored boreholes with 3-m interval, double-packer tests. Almost all of the major fracture zones within the site have been tested with interference tests, and the entire site has been subjected to multiple long-term pumping and tracer tests. Äspö is also the location of the Äspö Hard Rock Laboratory (HRL), an SKB research facility of tunnels and experiment galleries extending to a depth of 460 mbsl, with a total length of 3600 m. Mapping, testing, and sampling programs in the Äspö HRL have yielded important data, including the locations of otherwise undiscovered minor fracture zones.
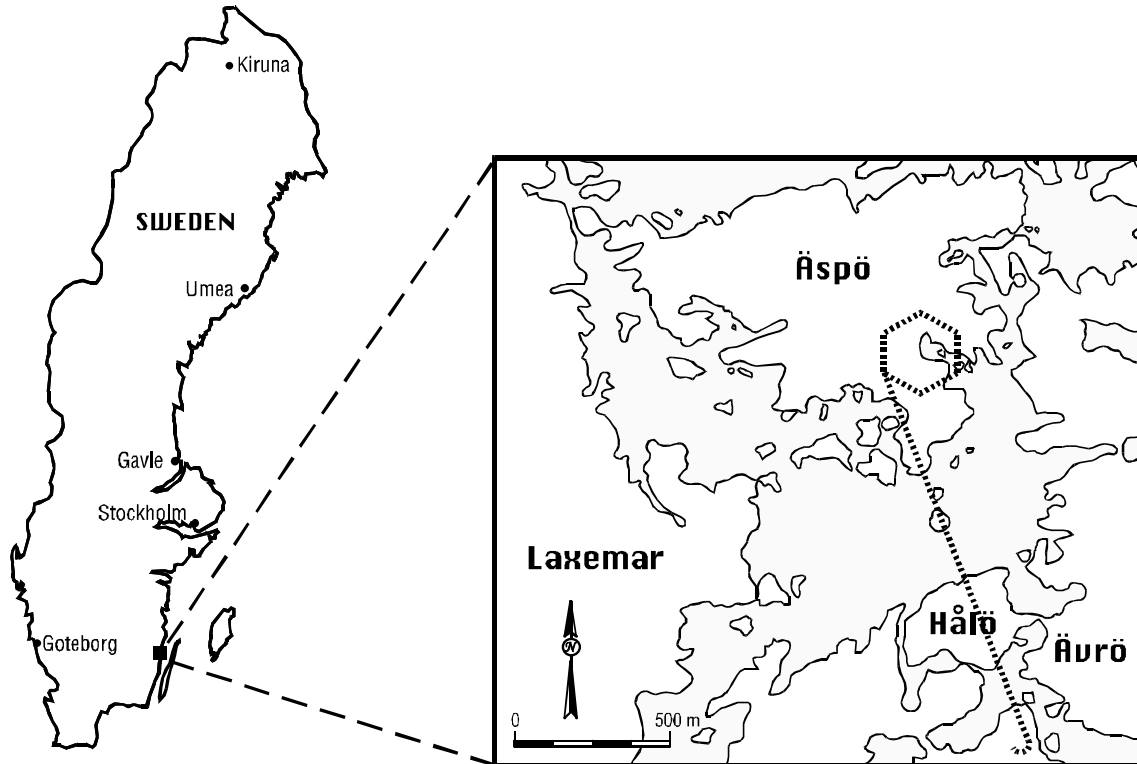
Figure 2-1. *Study site location. The tunnels of the Äspö Hard Rock Laboratory are shown as dotted lines.*

As part of studies at the Äspö Hard Rock Laboratory, /Rhén et al, 1997/ fitted an empirical relationship to the observed scale dependence of hydraulic conductivities interpreted for packer-test data at 3 metre, 30 metre, 100 metre, and full-length borehole tests (Figure 2-2). This yielded the following expression for the observed scale dependence of the geometric mean of hydraulic conductivities:

$$Log_{10}K_{gu} = Log_{10}K_{gm} + 0.782(Log_{10}L_u - Log_{10}L_m) \qquad (2\text{-}2)$$

where:

K_g = geometric mean of hydraulic conductivity (m/s)

L = length scale (m), assumed equal to the packer interval.

The subscripts m and u refer to the measurement and upscaled values, respectively. Although the confidence interval of the regression is wide, it suggests that geometric mean of hydraulic conductivity increases by more than an order of magnitude as the test scale increases from 3 m to 100 m (Figure 2-2). This empirical relationship is used to determine the conductivities for the regional model and is also used for one of the upscaling approaches; both are discussed in subsequent sections.
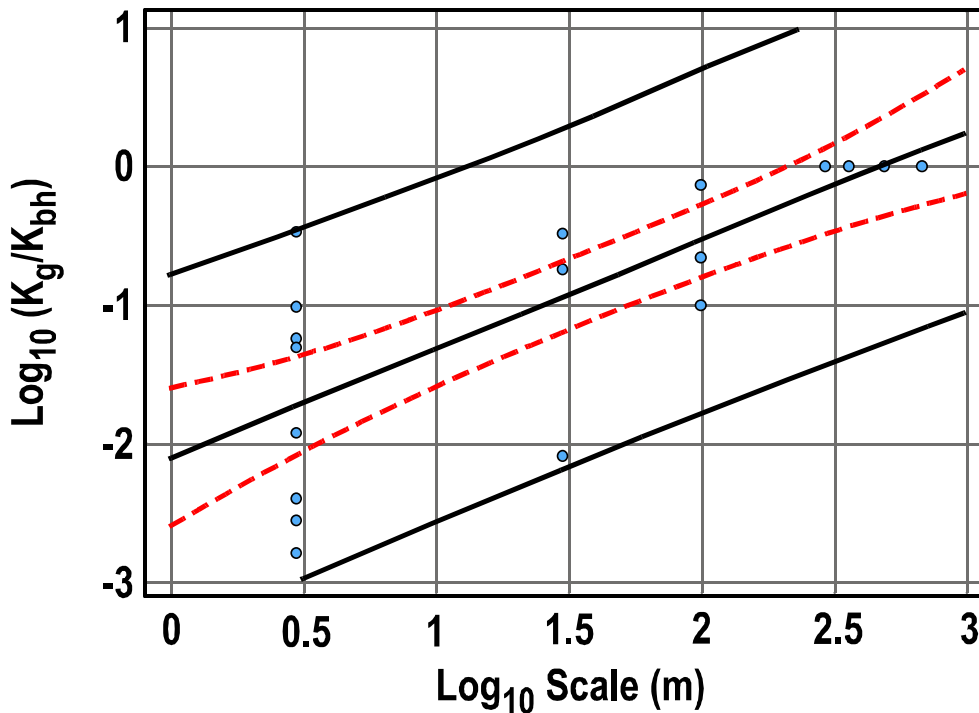
14

Figure 2-2. *Hydraulic conductivity scale dependence observed at Äspö HRL, showing the least-squares linear regression (central line), the 95 percent confidence intervals for the mean (inner pair of lines) and for prediction (outer pair of lines). The regression equation is $log_{10}K_g^{block} = log_{10}K_g^{test} + 0.782 (log_{10}L^{block} - log_{10}L^{test})$. Data points are K_g/K_{bh}, the geometric mean of test data of a given packer length, normalized by the full-borehole length test value /after Rhén et al, 1997/.*

The Aberg site-scale geostatistical model of hydraulic conductivity consists of the rock blocks described for SRD1 through 5, the SCD and a single variogram model. SR 97 (and this study) inferred a variogram model based on the 3-metre packer test data in the rock domain for both the SRD and SCD /Walker et al, 1997/. Unlike previous geostatistical studies of the Äspö data /La Pointe, 1994; Winberg, 1994; Niemi, 1995/, this study uses the interpreted hydraulic conductivities of /Rhén et al, 1997/ for the 3-metre packer tests. This is important because the Rhén interpretation has no lower measurement limit, a characteristic that can affect the statistics of the data. The interpreted conductivities are taken from cored boreholes KLX01, KAS02, KAS03, KAS04, KAS05, KAS06, KAS07 and KAS08, as found in the SKB database SICADA. The SKB code INFERENS was used to fit a model variogram and trends to the 3 m data /Walker et al, 1997/ using Iterative Generalized Least Squares Estimation /Neuman and Jacobsen, 1984/. The resulting model was an isotropic exponential model variogram, with a nugget of 1.48, a total variance of 2.84 and a practical range of 112 metres /Walker et al, 1997/. For an exponential model with this practical range and a nugget variance of 52 percent of the total variance, the integral scale reduces to 18 metres. Figure 2-3 shows the 3 m variogram estimates and the fitted model.
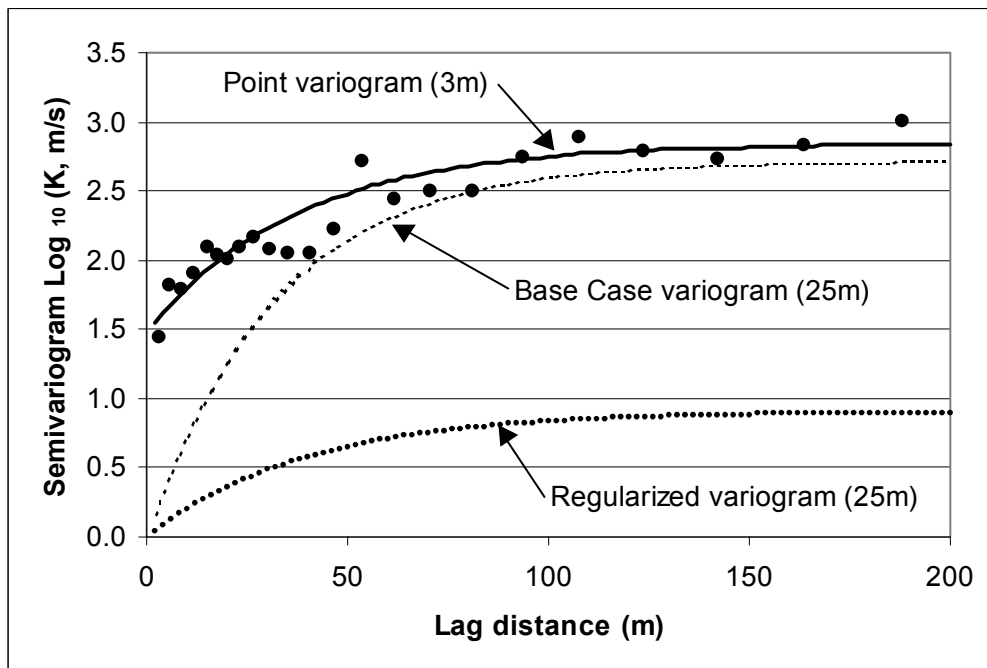
Figure 2-3. *Estimated, model, and regularised variograms for Aberg. The variogram estimates are based on the 3 m packer tests in the SRD. The Base Case variogram uses the Moye algorithm; the regularised variogram uses geostatistical regularisation, after /Journel and Huijbregts, 1978/.*

The hydraulic conductivities of the SCD are inferred from the interference tests conducted in each of the fracture zones. This type of test has a large tested volume, thus the medians of the test values in each fracture zone are assumed to be the K_e of each zone, with an approximate scale of 100 m. Interference tests are generally believed to be a more accurate measurement of hydraulic conductivity than single borehole packer tests, thus SR 97 used the interference tests to infer the SCD hydraulic conductivities rather than the 3 m packer tests. However, applying equation 2-2 to the median of the sparse 3 m packer tests in each SCD and upscaling to K_{100} yields approximately the K_e of each zone, suggesting that the inference is at least self-consistent with respect to scale. One consequence of is that the SR 97 approach must upscale the SRD conductivities, but downscale the SCD conductivities. The alternative methods simply use the inferred SCD values. The resulting parameters are summarised in Table 3-1.

HYDRASTAR has no facility for modelling spatially variable porosity or flow-wetted surface and thus these simply are scaling factors in this analysis, multiplied by the Darcy velocity to determine travel time and F-quotient (equation 2-1). Flow porosity is an uncertain parameter, whose value is thought to vary between 10^{-4} and 10^{-2} at this site; this study uses a conservative flow porosity value of $\varepsilon_f = 1 \times 10^{-4}$, with the sensitivity of the travel times to this value evaluated as part of the transport analysis. The flow-wetted surface is inferred from packer tests, with a uniform value of $a_r = 1.0 \text{ m}^2/\text{m}^3$ rock /Anderson et al, 1998/.

The design of the hypothetical repository is restricted by the occurrence of the fracture zones and the self-imposed requirement of limiting the waste-storage tunnels to the area beneath Äspö Island. The resulting design has two levels, with waste-storage tunnels at depths of 500 and 600 m /Munier et al, 1997/.

2.4 Model application

/Svensson, 1997/ used an integrated finite-volume continuum model, PHOENICS, to study Äspö regional flow, finding that the small net recharge combined with seawater intrusion produced a regional-flow pattern of recharge on inland areas with outflow to the Baltic Sea. This is consistent with hydraulic heads, salinities, and the observed locations of streams and mires. The /Svensson, 1997/ regional model included the density effects of seawater, but the site-scale modelling code, HYDRASTAR, cannot simulate density-dependent effects. Although this discrepancy might result in errors for the boundary heads specified for the site-model domain, the salinity of the Baltic Sea is low (approximately 1/7 that of normal seawater), and the freshwater-saltwater interface is believed to be stable. Consequently, for the purposes of SR 97, the /Svensson, 1997/ model was rerun with freshwater conditions to determine the regional-hydraulic heads, which are used as constant-head boundaries for the site-scale model.

The HYDRASTAR application consists of a 3-dimensional, regular grid of uniform, 25-metre spacing. The model grid covers an area of 2400 m by 2200 m, with a depth of 1250 m (approximately 6.6 km^3), and consists of 97 x 89 x 49 finite difference nodes. The prescribed head boundary conditions are adapted from the regional model by simple linear interpolation. The locations and geometries of the CD are deterministic, as defined by the geologic structural model for fracture zones of /Rhén et al, 1997/ (Figures 2-4 and 2-5). Figure 2-6 shows the representation of the SCD within the site-scale domain.

The model representation of the hypothetical repository uses 120 starting positions for flow paths as representative canister locations in each Monte Carlo realisation. The excavation-disturbed zone (EDZ) around each repository tunnel was not included, since the block dimensions of this grid are large (25 metres) relative to the narrow thickness of the EDZ (0.3 to 1.0 metres). The tunnel backfill material was assumed to have a hydraulic conductivity of 1 x 10^{-10} m/s. A brief examination of the number of realisations indicated that the median performance measures were approximately stable after 30 realisations; 50 realisations were used to insure stability. Additional details of the model application are given in /Walker and Gylling, 1998/.

Figure 2-4. *The Conductor Domain on the site scale (SCD) for the Äspö site, showing the tunnels of the Äspö Hard Rock Laboratory /from Rhén et al, 1997/.*
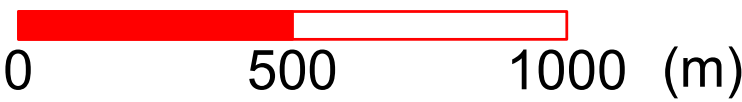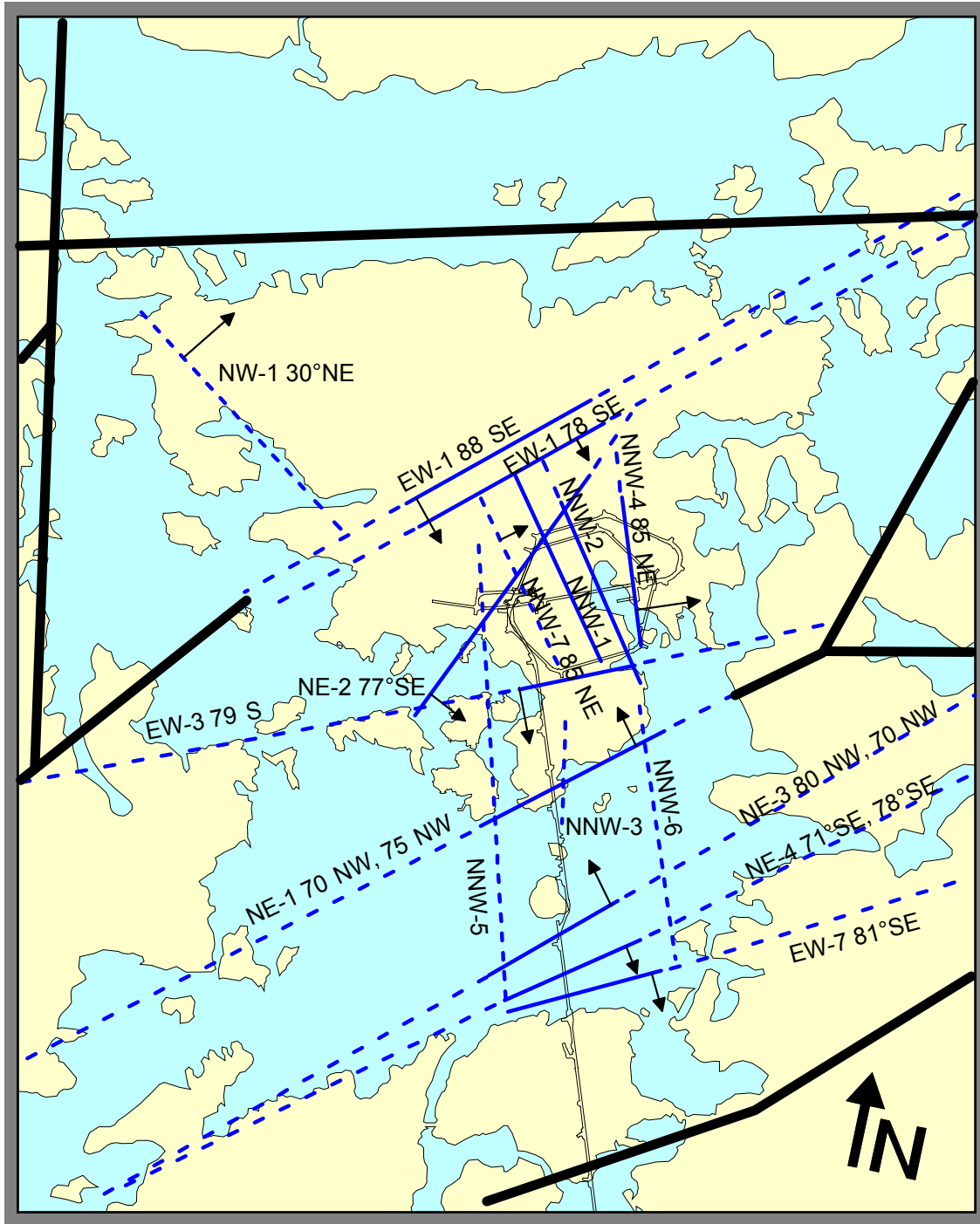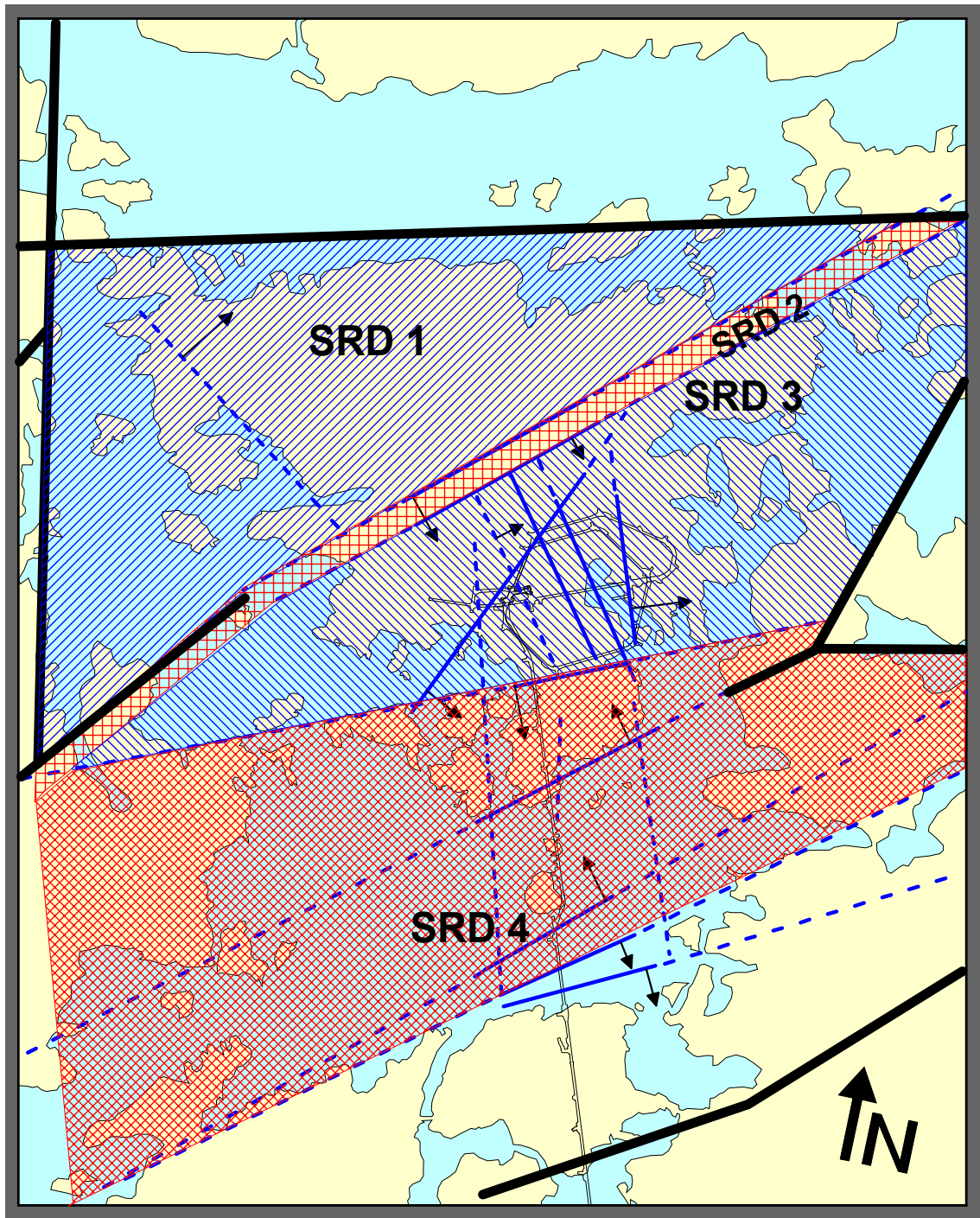
Figure 2-5. *The Rock Domain on the site scale (RCD) for the Äspö site, showing the tunnels of the Äspö Hard Rock Laboratory /from Rhén et al, 1997/.*
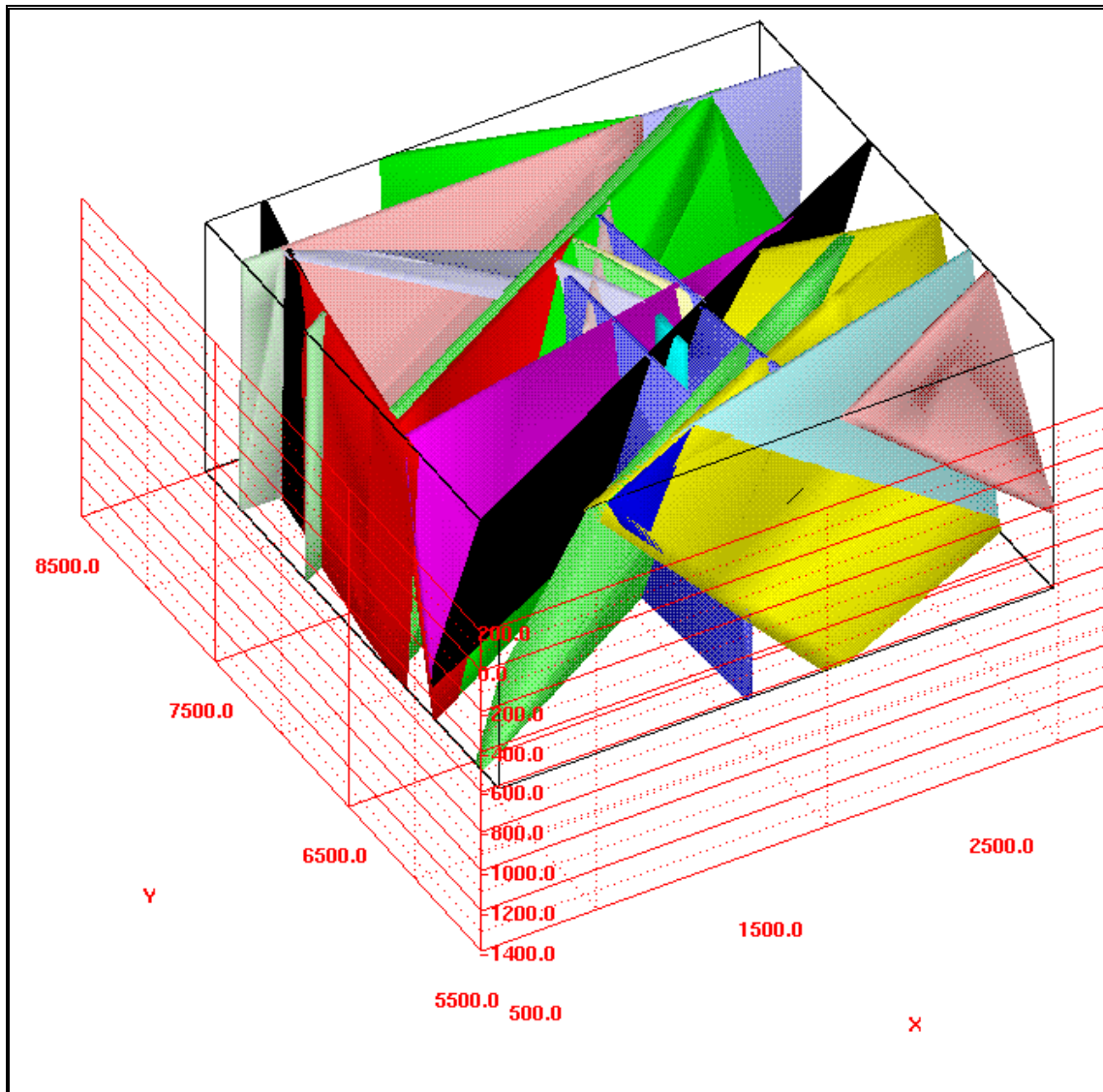
Figure 2-6. *HYDRASTAR representation of the fracture zones of the SCD, shown in oblique view from the Southwest.*

3   Upscaling approaches

The credibility of models within SR 97 required that their parameters be based on site-specific measurements, but the apparent scale dependence of hydraulic conductivity implies that small-scale measurements must be upscaled for use in larger-scale models. This upscaling should be appropriate for site conditions and adequately represent groundwater flow so that the performance assessment will be unbiased. However, upscaling of hydraulic conductivity is an active area of research, and the known upscaling approaches may not be appropriate for the sites examined by SR 97. Performance assessments for nuclear waste disposal routinely address unresolved uncertainties; this study applies the approach commonly used within performance assessments: apply the alternative methods to the same site, then compare the overall results to evaluate the impacts of the uncertainty /NEA, 1991/.

Upscaling approaches for numerical modelling can be divided into two general categories: those that upscale the distribution of the observed process and then simulate the block values, and those that simulate the observed process and then upscale the values falling in each block /Wen and Gómez-Hernández, 1996/. As noted in Section 2.1, HYDRASTAR is restricted to internally-generated fields of hydraulic conductivity at the block scale, and cannot use an externally generated field. This limits this study to considering upscaling approaches of the first category: upscale the observed distribution, then simulate the block-scale values. The built-in geostatistical simulation algorithm of HYDRASTAR generates multivariate, lognormally-distributed hydraulic conductivity fields, using planar trends to represent fracture zones. Thus, for this study, we transform the observed hydraulic conductivities as $Y = \log_{10}(K)$, and infer the mean of $\log_{10}$ conductivity, $\widetilde{Y}$, for each fracture zone and rock domain and a single, detrended variogram for Y. The upscaling methods adjust the inferred $\widetilde{Y}$ and variogram of Y to get the mean, $\widetilde{Y}_b$, and variogram Y_b of the block-scale $\log_{10}$ hydraulic conductivities

This study evaluates the range of upscaling uncertainties that can be evaluated within the current version of HYDRASTAR, but it should be noted that only the first category of upscaling approaches is examined. The second category, upscaling a dense simulation of conductivities, includes several robust numerical averaging schemes /McKenna and Rautman, 1996/ and renormalisation schemes that determine the full tensor of conductivity /e.g., Jackson et al, 2000/. The second category (numerical averaging or renormalization of a dense realisation) is computationally inefficient, but permits upscaling more general models of heterogeneity. Readers interested in additional information are referred to the excellent reviews of /Renard and de Marsily, 1997/, and /Wen and Gómez-Hernández, 1996/.

Various approaches have been developed for upscaling the distributional parameters of homogeneous, porous media /e.g., Indelman and Dagan, 1993b/, but upscaling for media with strong contrasts in hydraulic conductivity (fractured or bimodally distributed) is an active research area. This study examines upscaling for the case of nonstationary fractured media with domain-spanning fracture zones, a specific case that has received little attention. SR 97 evaluated upscaling for self-consistency by upscaling to coarser grid and recalculating the performance measures. The SR 97 approach was found to be approximately self-consistent, but only one approach was evaluated. /Holmén, 1997/ examined several upscaling methods for a similar performance assessment problem, but those methods have not yet been tested for the SR 97 problem.

The nested modelling approach of SR 97 requires 1) deterministic hydraulic conductivities for each fracture zone and rock domain in the regional-scale model, and 2) the mean and covariance of hydraulic conductivity for numerical blocks in the stochastic site-scale model. Ideally, these should be inferred from on-site measurements and preserve continuity (e.g., the boundary flows calculated by the regional and site-scale models should be equal over the boundaries of the site-scale domain). This study uses a single deterministic regional model, and then compares alternative methods of upscaling the hydraulic conductivity of the stochastic site-scale model. In addition to comparing upscaled parameters, the study runs the site-scale model to calculate the simplified measures of repository performance for each alternative. Flow balances between the regional- and site-scale models provide a check on the consistency of the upscaling of hydraulic conductivity.

3.1　Regional scale model

Hydraulic conductivities for the regional-scale model are chosen with the intent of providing the expected regional flux across the domain of the site-scale model. This is also the intent of the effective hydraulic conductivity of stochastic continuum mechanics, which is that value of K_e that satisfies:

$$\langle \vec{q} \rangle = -K_e \nabla \langle \vec{h} \rangle \qquad\qquad (3\text{-}1)$$

where $\langle \vec{q} \rangle$ is the expected flux across the site-scale domain, and $\nabla \langle \vec{h} \rangle$ is the expected gradient across the site-scale domain. This effective conductivity is, strictly speaking, valid only for an infinite, statistically homogeneous domain under uniform flow /Dagan, 1989/, but in practice these conditions are roughly satisfied for domains whose extent L_e is larger than eight to ten times the integral scale of the spatial covariance. The effective conductivity is useful for SR 97 in that it can be used to estimate the expected value of the flux over a domain /Rubin and Gómez-Hernández, 1990/.

The problem lies in determining K_e; one alternative is suggested by the observed scale dependency (equation 2-2). Unlike the analytical solutions of /Gutjahr et al, 1978/, the regression approach requires an explicit length scale for K_e, the effective conductivity of the point-scale observations. Geostatistical analyses of hydraulic conductivities

measured at Äspö suggest that the 3-m scale variogram (the point variogram) has an integral scale between 7 to 26 m /Niemi, 1995; LaPointe, 1994; Walker et al, 1997/. This suggests that the criteria $L_e > 10\lambda$ is approximately met for L_e on the order of 10^2 m. Observations of /Rhén et al, 1997/ qualitatively support this conclusion, since the standard deviation of $\log_{10} K$ approaches zero at approximately this measurement scale. It can be shown /Walker et al, 1997, appendix D/ that equation 2-2 gives results that are weakly comparable to the approximate solutions of /Gutjahr et al, 1978/, commensurate with the wide confidence interval of the regression (Figure 2-2).

/Svensson, 1997/ manually calibrated K_e for the upper surface and SRD 4 of the regional model by comparing observed and model results for hydraulic heads, the spatial distribution of recharge and discharge, and stream discharge. The regional model includes the decrease in conductivities with depth and conductive fracture zones to include the important effects of large-scale trends /Gelhar, 1993/. Thus the deterministic regional model for Aberg uses a set of effective hydraulic conductivities inferred as the 100-m scale value for the RRD and RCD (i.e., the K_{100} for each zone and region as determined by equation 2-2). These effective conductivities and the calibrated regional model have uncertainties, but this study neglects these uncertainties and considers the heads and boundary fluxes of the regional model to be completely known. This study thus only addresses the uncertainties of upscaling within the site-scale model.

The regional model of /Svensson, 1997/ lacked the resolution to represent the NNW individually. These zones were consequently represented as a single zone with hydraulic conductivity equal to the area-weighted arithmetic mean of the effective hydraulic conductivities of the represented zones. This is, of course, simply another upscaling algorithm, and may have consequences in the PA. However, the NNW zones have limited extent and thus have limited influence on the overall flow balance (this is evaluated in Section 4.1). Groundwater flow is roughly parallel to these zones, and in this situation the area-weighted arithmetic mean is known to be a rather good solution for the effective hydraulic conductivity of parallel layers. Thus, while this is an upscaling decision that may have consequences in PA, there are reasons to suspect that the impacts are on the order of the variations seen in the analysis of sensitivity to minor changes in zone properties (Section 4.1). Likewise, the K_e is also just another estimate, and its uncertainty should be evaluated as well. Such additional analyses are beyond the scope of the current report.

3.2   Site-scale model

The HYDRASTAR models of SR 97 attempt to represent all the fracture zones of the SCD, but in practice, several zones are narrower than the grid spacing of 25 m: EW 3 and 7, NE-2, NW-1, the SFZ, and all NNW zones. To retain these important features, the HYDRASTAR representation increased the zone widths to 25 m and decreased the hydraulic conductivities proportionately to preserve each zones' transmissivity. In reality, this is another upscaling, one that is not evaluated by this study. However, as noted above regarding the representation of the NNW zones in the regional model, the narrower zones contribute little to the overall flow balance and the corrections to the hydraulic conductivity are small relative to the upscaling adjustments of the various

methods. Therefore, while this upscaling decision may have consequences in the PA that should be evaluated, there are reasons to suspect that the impacts are on the order of the variations seen in the analysis of sensitivity to minor changes in zone properties (Section 4.1).

3.2.1   Upscaling in SR 97

In the SR 97 hydrogeologic modelling studies, the Aberg site-scale model addressed the scale dependency of hydraulic conductivity using the observed scale dependency (Figure 2-2) and numerical regularisation to upscale the variogram of conductivity. Thus, SR 97 used equation 2-2 to upscale the mean of the $\log_{10}$ hydraulic-conductivity measurements to the mean of the numerical model block $\log_{10}$ hydraulic-conductivity distribution for each SRD and SCD. The results of these calculations are presented in Table 3-1.

The block-scale variogram model for this method is estimated by first regularising each 3 m measurement to 25 m via an analytical solution based on Moye's formula for double-packer hydraulic tests /Moye, 1967/. In effect, the regularised value of each 3 m test is the arithmetic mean of measurements falling within a 25 m window, corrected for packer length and borehole radius /Norman, 1992/. The common logarithms of the regularised measurements are fitted with a trend and variogram model using iterative generalized least-squares estimation /Neuman and Jacobsen, 1984/. Figure 2-3 presents the resulting regularised variogram: an isotropic exponential model variogram, with zero nugget, a total variance of 2.72 and a practical range of 97 metres (integral scale of 32 metres) /Walker et al, 1997/.

3.2.2   Alternative Method I: SCD as 2-dimensional features

Similar to the SR 97, the first alternative upscaling approach uses observed scale dependence (equation 2-2) to determine the mean $\log_{10}$ hydraulic conductivity, and Moye's regularisation for the variogram. However, the SCD generally have a large contrast in conductivity with the surrounding SRD (almost 2 orders of magnitude) and are thin relative to their lateral extent. This alternative assumes that the SCD may be approximated as 2-D media, such that the stochastic continuum solution of $K_e = K_G$ applies /Matheron, 1967/. Since for the SCD the effective conductivity is inferred from the large-scale interference tests of 100-m scale ($K_e = K_{100}$), this results in $\widetilde{Y}_b = \log_{10}(K_{100})$. Relative to the upscaling approach used in SR 97, this increases the $\widetilde{Y}_b$ of all the SCD; there is otherwise no difference with respect to the SR 97 approach (Table 3-1).

Table 3-1. Parameters for Base Case model and Alternative Methods. Below 600 mbsl, all hydraulic conductivities reduced by a factor of 1/10. The flow rates are the net flow through the site model surfaces (m^3/s x 10^{-3}).

Unit	Width (m)	Regional Model (100 m)	SR 97 Base	Base Rerun	Updated Base	I	II	III
			SR 97 Approach			Alternative Methods		
EW-1N	30	–7.30	–7.79	–7.79	–7.79	–7.30	–7.30	–7.30
EW-1S	30	–6.13	–6.62	–6.62	–6.62	–6.13	–6.13	–6.13
EW-3	15	–5.80	–6.50	–6.50	–6.50	–6.02	–6.02	–6.02
EW-7	10	–5.17	–6.05	–6.05	–6.05	–5.57	–5.57	–5.57
NE-1	30	–5.00	–5.48	–5.48	–5.48	–5.00	–5.00	–5.00
NE-2	5	–7.09	–8.27	–8.27	–8.27	–7.79	–7.79	–7.79
NE-3	50	–5.24	–5.72	–5.72	–5.72	–5.24	–5.24	–5.24
NE-4	40	–6.12	–6.61	–6.61	–6.61	–6.12	–6.12	–6.12
NNW-1	20	–6.26	–6.84	–6.84	–6.84	–6.36	–6.36	–6.36
NNW-2	20	–5.55	–6.13	–6.13	–6.13	–5.65	–5.65	–5.65
NNW-4	10	–4.82	–5.71	–5.71	–5.71	–5.22	–5.22	–5.22
NNW-5	20	–7.00	–7.58	–7.58	–7.58	–7.10	–7.10	–7.10
NNW-7	20	–6.62	–7.20	–7.20	–7.20	–6.72	–6.72	–6.72
NNW-8	20	–6.30	–6.88	–6.88	–6.88	–6.40	–6.40	–6.40
NW-1	10	–7.77	–8.65	–8.65	–8.65	–8.17	–8.17	–8.17
NNW-3	20	–6.00	–6.79	–6.79	–6.58	–6.10	–6.10	–6.10
NNW-6	20	–6.15	–6.79	–6.79	–6.74	–6.25	–6.25	–6.25
SFZ-w*	20	–6.82	–7.41	–7.41	–7.41	–6.92	–6.92	–6.92
SFZ-ww**	20	–5.30	–5.88	–5.88	–5.88	–5.40	–5.40	–5.40
SRD 1		–7.55	–8.03	–8.03	–8.02	–8.02	–7.90	–8.00
SRD 2		–6.63	–7.11	–7.11	–7.10	–7.10	–6.98	–7.08
SRD 3		–8.28	–8.76	–8.76	–8.75	–8.75	–8.63	–8.73
SRD 4		–7.05	–7.54	–7.54	–7.54	–7.54	–7.40	–7.50
SRD 5		–7.13	–7.61	–7.61	–7.60	–7.60	–7.48	–7.58
SRD - other		–8.07	–8.54	–8.54	–8.54	–8.54	–8.42	–8.52
Variance		0	2.72	2.72	2.72	2.72	0.909	0.909
Integral Scale		N/A	32.3	32.3	32.3	32.3	39.2	39.2
Total Inflow		17.4	8.11	8.60	8.65	19.17	5.70	***
Total Outflow		18.1	8.11	8.57	8.63	19.16	5.73	***
Balance (In-Out)		–0.675	– 0.0037	0.0248	0.0255	0.0063	0.0326	***

*   For regional SFZ zones denoted w.

**   For regional SFZ zones denoted ww.

*** The upscaled parameters of Method III are nearly identical to those of Method II, and thus Method III was not carried through the Monte Carlo simulations.

3.2.3   Alternative Method II: Effective conductivities

Similar to /Holmén, 1997/, we might use one of the approximate solutions for K_e, the effective conductivity of the domain, to determine $\widetilde{Y}_b$. For example, the 1st order perturbation of /Gutjhar et al, 1978/ is given by:

$$K_e = K_G \left[1 + \left(\frac{1}{2} - \frac{1}{n} \right) \sigma_{\ln K}^2 \right] \qquad (3\text{-}2)$$

/Gelhar and Axness, 1983/ conjectured that this was the first two terms of the Taylor series expansion of the conjecture of /Matheron, 1967/:

$$K_e = K_G \exp \left[\left(\frac{1}{2} - \frac{1}{n} \right) \sigma_{\ln K}^2 \right] \qquad (3\text{-}3)$$

which for three-dimensional media reduces to:

$$K_e = K_G \exp \left[\sigma_{\ln K}^2 \middle/ 6 \right] \qquad (3\text{-}4)$$

/Dagan, 1993/ showed that equation 3-4 was correct to the 2nd order perturbation in σ^2_{lnK}. For use in upscaling, we might rearrange equation 3-4 as:

$$\widetilde{Y}_b = \log \left[\frac{K_e}{\exp \left[\sigma_{\ln Kb}^2 \middle/ 6 \right]} \right] \qquad (3\text{-}5)$$

which has assumed that the discretisation of the domain is fine enough that the blocks are effectively point values. As discussed in Section 3.1, we estimate K_e via the large-scale borehole tests; what remains now is to estimate the block-scale variance $\sigma_{\ln Kb}^2$. /Holmén, 1997/ addresses this by simultaneously regressing nonlinear equations to the Äspö data for Y and σ^2_{lnK} versus the test scale, linking the regressions via the solution for the effective conductivity (equation 3-4). /Holmén, 1997/ did not upscale the integral scale of the variogram, asserting that the correlation is weak and thus spatial correlation is negligible. While this may be true for flow, it is not true for the macrodispersivity, which is directly proportional to the integral scale /Gelhar and Axness, 1983/.

As a modification of /Holmén, 1997/, Alternative Method II uses geostatistical regularisation to upscale the point variogram to a variogram for the numerical blocks. The sill of the regularised variogram is an estimate of the variance of Y_b, which then is used in equation 3-5 to estimate $\widetilde{Y}_b$. Thus, for the SRD, we: 1) infer K_G and σ^2_{lnK} from

the statistics of the 3 m data falling in each SRD; 2) estimate K_e for each SRD from equation 2-2 at 100 m; 3) estimate the 25 m-scale variogram of Y_b by applying geostatistical regularisation /Journel and Huijbregts, 1978/ to the variogram of $\log_{10} K$ inferred from the 3 m data (Section 2.3); and 4) substitute these estimates of $\sigma^2_{\ln Kb}$ and K_e into equation 3-5 to estimate $\widetilde{Y}_b$ for each SRD (note that the sill of the regularised $\log_{10}$ variogram of hydraulic conductivities, σ^2_{Yb}, is transformed to natural logarithms to get $\sigma^2_{\ln Kb}$ for use in equation 3-5). For the SCD, assume that (as in Alternative 1) the SCD are two-dimensional media with $K_e = K_{100} = K_g$, and thus $\widetilde{Y}_b = \log_{10} K_{100}$.

The variogram regularisation uses FORTRAN codes adapted from /Journel and Huijbregts, 1978/ (see also Appendix A). Figure 2-3 presents the resulting 25 m-block-regularised model variogram, which is an exponential model with zero nugget, a total variance of 0.91, and a practical range of 118 m (integral scale of 39 m). The total variance of the regularised variogram is substituted into equation 3-5 to estimate $\widetilde{Y}_b$ for the SRD. Results for this calculation are presented in Table 3-1.

As discussed in Appendix A, geostatistical regularisation of the variogram removes the nugget variance in a nearly linear fashion. In effect, the nugget is subtracted from the variogram model and the remaining transitional model is regularised, such that, the larger the nugget, the lower the total variance of the regularised model (compare the 3-m model and 25-m regularised models of Figure 2-3). In this study, the nugget variance large, resulting in a large decrease in the upscaled variance and a consequent increase in the upscaled hydraulic conductivities (equation 3-5). This implies that this upscaling method (and Alternative Method III) may be sensitive to the inference of the model of the point variogram.

3.2.4   Alternative Method III: Stochastic continuum mechanics

The upscaling methods outlined above are developed either from the observed scale dependence or borrowed from solutions for effective conductivities or from analytical solutions for well hydraulics. Thus, although such methods are conceptually sensible, they are not derived analytically from first principles. Alternative Method III considers the possibility that an analytical solution for upscaling might result in hydraulic conductivities that would lead to a dramatically different conclusion regarding the repository performance.

Several authors have presented analytical upscaling methods for the upscaled mean and variogram of block hydraulic conductivities. /Rubin and Gómez-Hernández, 1990/ presented a solution for the upscaled mean and covariance of a 2-dimensional lognormal transmissivity field. /Pozdniakov and Tsang, 1999/ derive a semianalytical solution for the upscaled mean and variance (but not the spatial correlation) in three dimensions. For the present study, the most useful solution appears to be that of /Indelman and Dagan, 1993a,1993b/, /Indelman, 1993/, and /Indelman and Dagan, 1993c/, hereinafter referred to as P1, P2, P3, and P4. In that series of papers, Indelman and Dagan present a 1st-order perturbation solution for the upscaled mean and

autocorrelation of block conductivity. Their solution is rigorously derived and quite general (1, 2, or 3 dimensions, arbitrary block shape and anisotropic media), but it assumes that the hydraulic conductivities are of low variance ($\sigma^2_{\ln K} < 1.0$). None of these analytical approaches address the weakly lognormal, nonstationary, fractured media considered by SR 97, and thus these analytical solutions are not necessarily more appropriate than the heuristic methods described in Sections 3.2, 3.3, and 3.4. In spite of these limitations, the Indelman and Dagan solution is the only known analytical solution for the upscaled mean and variogram of block conductivities in a 3-dimensional domain.

The /Indelman and Dagan, 1993b/ approach reduces to a set of integral equations for the upscaled mean, variance, and autocorrelation of block conductivities. For a statistically isotropic media, P3 gives the geometric mean of block conductivities as:

$$\widetilde{K}_G = \frac{\left[1 + \left(\frac{1}{2} - \frac{1}{n}\right)\sigma^2_{\ln K}\right]}{\left[1 + \left(\frac{1}{2} - \frac{1}{\widetilde{a}_i}\right)\sigma^2_{\ln Kb}\right]} K_G \tag{3-6}$$

and P2 gives the variance as:

$$\sigma^2_{\ln Kb} = \frac{\sigma^2_{\ln K}}{\omega^2} \int \rho_{\ln K}(\vec{r}) H(\vec{r}) d\vec{r} \tag{3-7}$$

and the autocorrelation as:

$$\rho_{\ln Kb}(\vec{r}) = \frac{\sigma^2_{\ln K}}{\sigma^2_{\ln Kb}\omega^2} \int \rho_{\ln K}(\vec{r}') H(\vec{r} - \vec{r}') d\vec{r}' \tag{3-8}$$

where

$$\widetilde{a}_i = \frac{1}{(2\pi)^{n/2}} \int \frac{k^2_i}{k^2} \hat{\rho}_{\ln K}(\vec{k}) d\vec{k} \tag{3-9}$$

$$\frac{H(r)}{\omega^2} = \begin{cases} \frac{1}{abc}\left(1 - \frac{|r_1|}{a}\right)\left(1 - \frac{|r_2|}{b}\right)\left(1 - \frac{|r_3|}{c}\right) & for \quad |r_1| < a, |r_2| < b, |r_3| < c \\ \\ 0 & otherwise \end{cases} \tag{3-10}$$

where $\omega = abc$, with a, b, and c being the lengths of the sides of the numerical blocks; and $\hat{\rho}_{\ln K}(\vec{k})$ is the Fourier transform with respect to k of the autocorrelation of $\ln K$; n is the number of dimensions. For any anisotropic element (i.e., any shape other than spherical), equation 3-6 indicates that the block conductivity will be an anisotropic tensor. Except for a few cases, equations 3-7, 3-8, and 3-9 must be evaluated numerically. The approach has been used occasionally /e.g., Ritzi et al, 2000/, but no evaluations of its accuracy or range of validity were uncovered during the literature review.

In practice, P3 (Figure 3) shows that the results for cubical and spherical blocks are nearly indistinguishable; if the variogram is isotropic for spherical blocks, P4 (equation 37) shows that equation 3-9 reduces to $\widetilde{\alpha}_i = 1/n$ for all i directions. Thus, with little loss in accuracy, equation 3-6 reduces to:

$$\widetilde{K}_G = \frac{\left[1 + \left(\dfrac{1}{2} - \dfrac{1}{n}\right)\sigma_{\ln K}^2\right]}{\left[1 + \left(\dfrac{1}{2} - \dfrac{1}{n}\right)\sigma_{\ln Kb}^2\right]} K_G \tag{3-11}$$

and the numerical integration of equation 3-9 is unnecessary. For integral 3-7, we observe that it is the geostatistical regularisation of the autocorrelation within the numerical block ω /Dagan, 1989, section 1.9/. Using the identities provided by /Journel and Huijbregts, 1978, p 78/ it is easy to show that equation 3-7 is total variance of the regularised variogram calculated for Alternative Method II. Similarly, the integral 3-8 is the regularisation of the autocorrelation between numerical blocks ω, separated by distance r, and thus the autocorrelation of equation 3-8 is a trivial rescaling of the regularised variogram calculated previously for Alternative Method II.

/Pozdniakov and Tsang, 1999/ suggest that the exponential conjecture of /Gelhar and Axness, 1983/ could be used to extend first-order perturbation solutions such as equation 3-11 to the case of larger variances. We likewise conjecture that the true solution for upscaling in 3-D for isotropic media with spherical blocks is:

$$\widetilde{K}_G = \frac{\exp\left[\sigma_{\ln K}^2 / 6\right]}{\exp\left[\sigma_{\ln Kb}^2 / 6\right]} K_G \tag{3-12}$$

Dagan's proof for equation 3-4 /Dagan, 1993/ is not necessarily applicable to equation 3-12, and thus there is no proof that this conjecture is equally valid. However, similar to /Pozdniakov and Tsang, 1999/, we argue that this conjecture seems no less plausible here than for equation 3-4. Since Alternative Method II uses the exponential conjecture of equation 3-4, using this conjecture in Alternative Method III would be consistent. Given these arguments, Alternative Method III will use exponential conjecture to extend equation 3-11 to equation 3-12.

Similar to Alternative Method I, this method will assume that the SCD are 2-D features and the SRD are 3-D features, and thus Alternative Method III uses the corresponding 2-D and 3-D forms of the equations. For 2-dimensional media, equation 3-11 reduces to $\widetilde{K}_b = K_G$, and since we infer $K_G = K_{100}$, Alternative Method III will use $\widetilde{Y}_b = \log_{10}(K_{100})$ for the SCD. Although equation 3-7 and 3-8 reduce to 2-dimensional regularisation for a 2-dimensional domain, this method infers the variogram from three-dimensional regularisation of the variogram of the 3 m data falling within the SRD (as discussed in Section 2.3, HYDRASTAR can accept a single model variogram only).

In summary, Alternative Method III computes the block mean, variance and variogram for the SRD via the 3-dimensional forms of equations 3-7, 3-8, and 3-11; equations 3-7 and 3-8 effectively are the regularised variance and variogram computed in Alternative Method II. For the SCD, the block mean reduces to $\widetilde{Y}_b = \log_{10}(K_{100})$ with the same variance and variogram as the SRD. Thus, Alternative Method III uses the same variogram and SCD values as Method II; only the SRD values will differ (Table 3-1). We note that these values are little different than those of Alternative Method II, and thus we expect little difference in the performance measures. Consequently, this study proceeds no further with Alternative Method III.

4 Results

The previous section introduced each of the upscaling methods examined in this report, and presented the results of the upscaling calculations for the Base Case scenario of the hypothetical Aberg repository. For each method, these results were a set of block-scale geometric mean for each hydraulic unit and the block-scale variogram of $\log_{10}$ hydraulic conductivity. This section presents the Monte Carlo simulations that use these upscaled parameters, consisting of 50 realisations of the hydraulic conductivity field, each with 120 flowpath starting positions as representative canister positions. HYDRASTAR solves a system of equations for groundwater flow in each of the realisations, and then uses a particle-tracking algorithm to determine the travel time and flow paths. Statistics for the simplified performance measures of travel time, canister flux, and F-quotient are computed over all realisations for the entire set of flow paths.

As has been discussed in SR 97, the model simulations are slightly influenced by the input parameter that controls the maximum simulation time for particle tracking. This maximum time can influence the result because a few particles will fail to exit the upper surface of the model domain (to the accessible environment) before the simulation is abandoned. Some of these particles are trapped in stagnant zones deep in the model, and fail to move; others exit the lateral sides of the model, and their travel times are arbitrarily set to the maximum time (100,000 years, in these simulations). Typically, less than one percent of all particles will fail to exit the upper surface of the Aberg site-scale model domain, forming a small set of outliers that has only a limited influence on the statistics. For the sake of consistency with SR 97, the statistics for the canister flux are compiled for the full set of particles, while the statistics for the travel time and F-quotient are compiled with the failed particles deleted.

4.1 The SR 97 approach

As discussed in Section 3.2.1, SR 97 addressed the upscaling of mean hydraulic conductivity using the observed scale dependency of hydraulic tests and a numerical regularisation to determine the covariance of block conductivity. Before proceeding with the analysis, we should note that the Aberg Base Case as presented in this study is slightly different from that presented by /Walker and Gylling, 1998/ for the Aberg Base Case in SR 97. Some of these differences are minor changes in the computations, while others are potentially more important. The first two Monte Carlo simulations repeat the Aberg Base Case of SR 97 with just these changes so that we may isolate their effects from those of changing the upscaling methods.

The first simulation repeats the Aberg Base Case using the SR 97 approach, to verify that minor computational changes have had little effect on the performance measures. Relative to SR 97, this analysis: 1) uses a different computer platform; 2) uses 50 realisations where SR 97 used 100 realisations; 3) compiles boundary flow statistics for 50 realisations where SR 97 used five realisations; and 4) uses a maximum travel time

of 100,000 years where SR 97 used 10,000 years. The Monte Carlo simulation associated with these minor changes is referred to as the Aberg Base Case Rerun, or simply 'the Rerun'. The simulations are otherwise identical to the Aberg Base Case presented in SR 97 /Walker and Gylling, 1998/. Table 4-1 presents the performance measures and boundary fluxes for the Rerun, with just 0.5 percent of the particles failing to exit the upper surface of the model. In comparison to the SR 97 results, the statistics of the performance measures are relatively insensitive to the combined affects of these minor computational changes. This comparison also suggests that the Monte Carlo estimates of the boundary fluxes, variances, and percentiles are relatively stable.

A second simulation evaluates the impact of updating inferred values for two of the SCD, zones NNW-3 and NNW-6. A review of the inference for these zones revealed that the effective hydraulic conductivities of /Rhén et al, 1997, Table A2-7/ differed from those used in SR 97 /Walker and Gylling, 1998, Table 3-1/. This study used the effective hydraulic conductivities of Rhén et al for zones NNW-3 and NNW-6, resulting in an increase in $\log_{10}$ hydraulic conductivity of 0.2 and 0.06, respectively (Table 3-1). The simulation of the updated Aberg Base Case, or simply 'the Update', is otherwise identical to the Rerun (50 realisations, new platform). Table 4-1 presents the statistics of the performance measures, with just 0.4 percent of the particles failing to exit the upper surface of the model. The Update has a median travel time 10.7 years, slightly shorter than that of the Rerun (10.8 years). The differences between these and the other statistics of the Update and the Rerun are less than the differences between those of SR 97 and the Rerun. This suggests that the impacts of updating the hydraulic conductivities of NNW-3 and NNW-6 are negligible within the context of this study.

Table 4-1. Statistics for the Aberg Base Case using the SR 97 Method: the SR 97 Base Case, the Rerun, and the Update. Statistics for t_w and the F-quotient are calculated with only the path lines exiting at the upper boundary, and q_c statistics are calculated with the entire set of pathlines. A flow porosity of $\varepsilon_f = 10^{-4}$ and a flow-wetted surface of $a_r = 1.0$ m^{-1} are used to calculate t_w and the F-quotient.

	SR 97		The Rerun		The Update		
	$\text{Log}_{10} t_w$	$\text{Log}_{10} q_c$	$\text{Log}_{10} t_w$	$\text{Log}_{10} q_c$	$\text{Log}_{10} t_w$	$\text{Log}_{10} q_c$	Log_{10} F-quotient
Mean	1.069	–2.799	1.086	–2.813	1.082	–2.806	5.082
Median	1.015	–2.736	1.035	–2.751	**1.028**	**–2.744**	**5.028**
Variance	0.599	0.935	0.606	0.949	**0.613**	**0.946**	**0.613**
5th percentile	–0.125	–4.479	–0.119	–4.524	–0.131	–4.515	3.869
25th percentile	0.533	–3.430	0.554	–3.447	0.539	–3.444	4.539
75th percentile	1.563	–2.114	1.577	–2.124	1.574	–2.115	5.574
95th percentile	2.431	–1.298	2.456	–1.319	2.456	–1.314	6.456
Net Flow Through Site Model Surfaces (m^3/s x 10^{-3})							
Total Inflow	8.11		8.60		8.65		
Total Outflow	8.11		8.57		8.63		
Mass balance (In-Out)	–0.0037		0.0248		0.0255		

This updated Aberg Base Case forms the reference case for comparisons in the remainder of this study, and thus it is examined in somewhat greater detail than the Rerun. Figure 4-1 presents the cumulative median $\log_{10}$ travel time versus the number of realisations; the median is approximately stable after 30 realisations, with a statistical fluctuation of approximately 0.5 yr. Figure 4-2 presents a similar plot for the median $\log_{10}$ canister flux: it is also approximately stable after 30 realisations, with a statistical fluctuation of approximately 0.04×10^{-3} m/yr (similar analyses of Monte Carlo stability for the other upscaling methods yield similar results; they are not presented in this report). As reported in Table 4-1, the median travel time is 10.7 years with a log-scale variance of 0.613; the median canister flux is 1.80×10^{-3} m/yr with a log-scale variance of 0.946; and the median F-quotient of 1.07×10^{5} yr/m with a log-scale variance of 0.613.
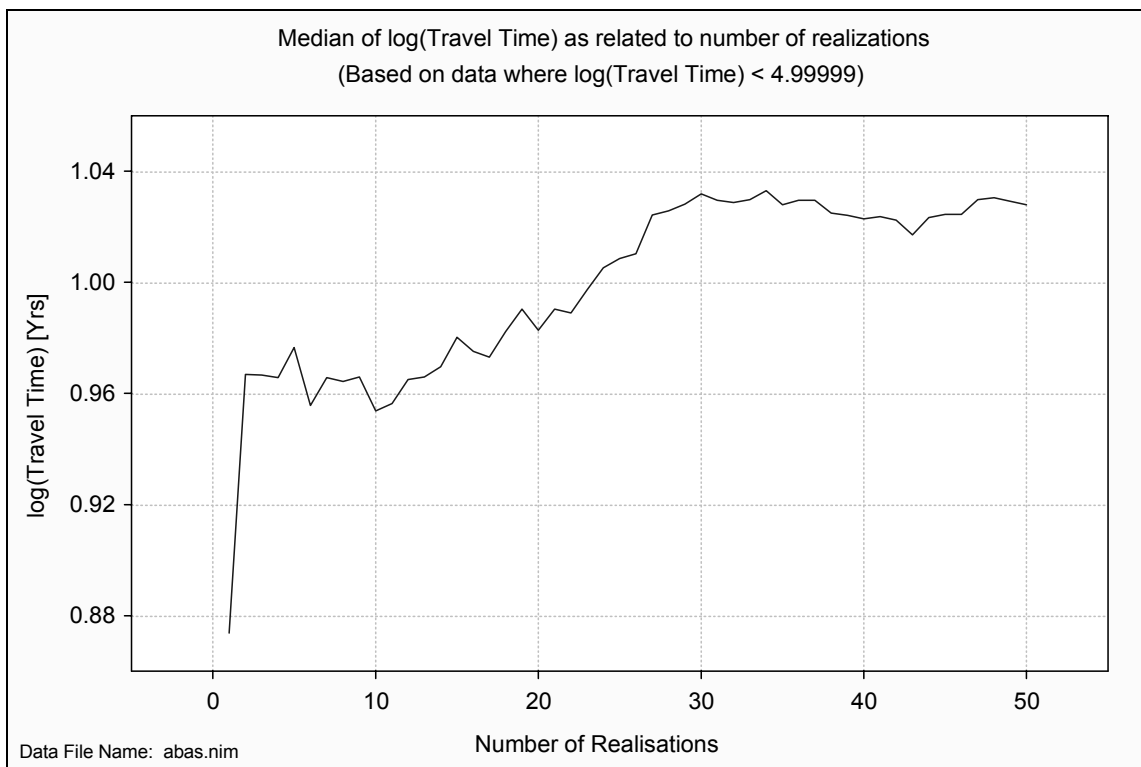

Figure 4-1. *Monte Carlo stability in the Aberg Updated Base Case. Median travel time versus number of realisations. Results for 120 starting positions and a flow porosity of $\varepsilon_f = 1x10^{-4}$.*
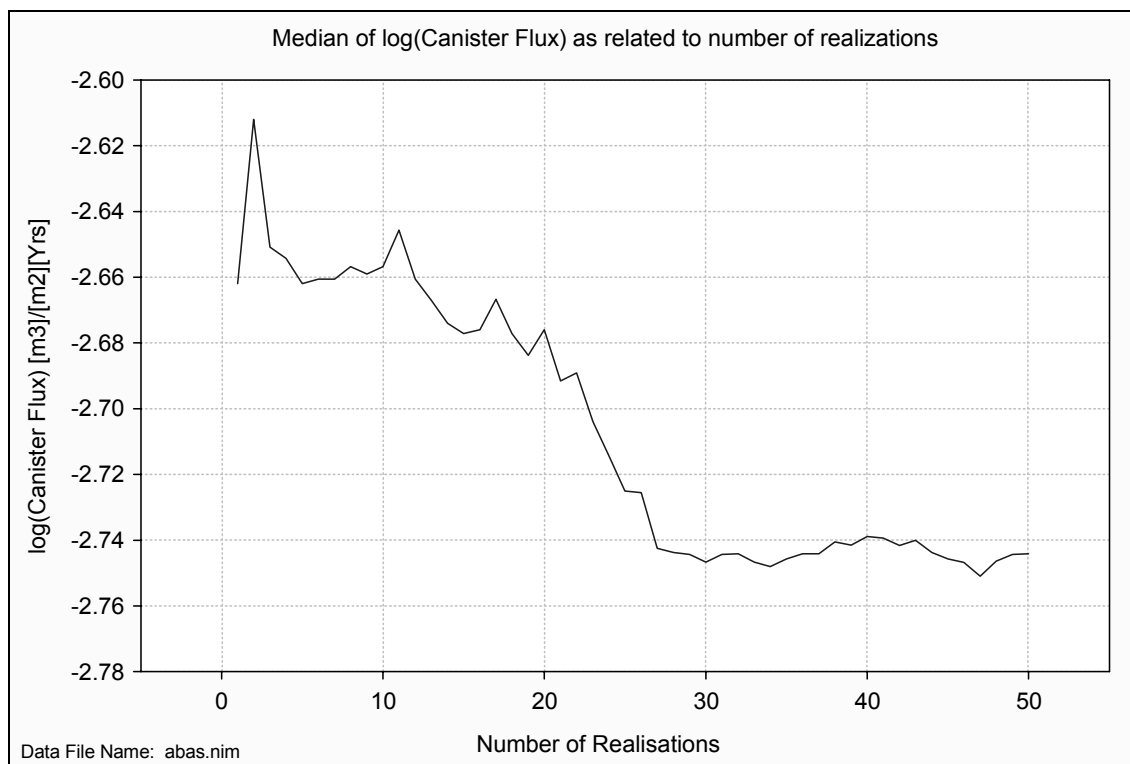
Figure 4-2. *Monte Carlo stability in the Aberg Updated Base Case. Median canister flux versus number of realisations. Results for 120 starting positions.*

Table 4-2 presents the net flow over each boundary of the site-scale domain for the Rerun versus those of the regional model. The majority of the inflow to both domains comes from the west, and the majority of the outflow is directed out the upper surface of the domains to the Baltic Sea. This is consistent with the regional pattern of recharge and discharge /Svensson, 1997/. The boundary flows of the site model are approximately ½ those of the regional model.

Figure 4-3 presents the frequency histogram of the common logarithm of travel time for 50 realisations, each with 120 starting positions as representative canister locations. The outliers seen at the upper tail of the histogram (approximately 0.4 percent) are particles that fail to exit the upper surface of the model and thus receive the default maximum travel time of 100,000 years. Figure 4-4 is a box plot of the number of realisations with travel times less than one year, versus starting position number. Starting positions between 13 through 19, 41 through 60, 74 through 81, and 99 through 120 seem to be less favourable, since starting positions in this location have several realisations with travel times less than one year. As noted in the SR 97 report /Walker and Gylling, 1998/, these starting positions are in SRD 2 and SRD 4, whose hydraulic conductivities are higher than the other SRDs (Table 3-1).

34

Table 4-2. Boundary flow consistency for Updated Aberg Base Case, regional model versus site-scale model.

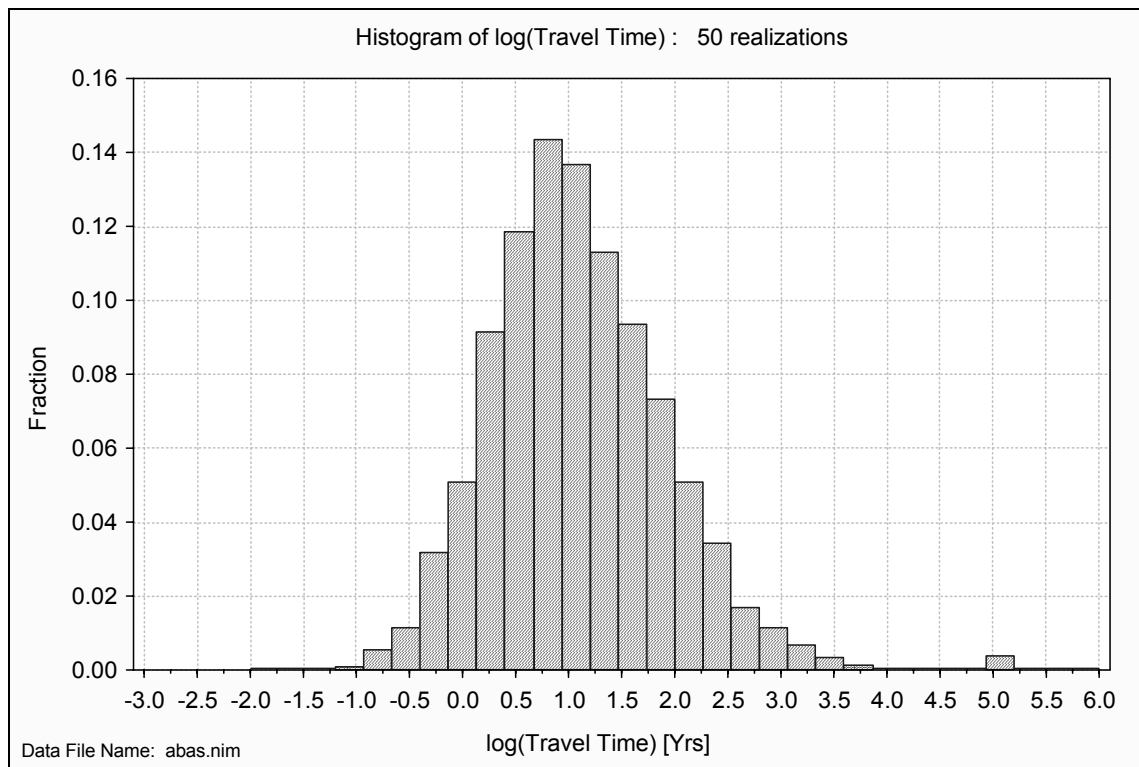| Model Surface	Net Flow Through Site Model Surfaces (m³/s x 10⁻³)			
	Regional Model		Site-Scale Model Updated Base Case	
West	13.7	In	5.43	In
East	0.916	In	1.15	In
South	1.81	In	0.698	In
North	0.625	In	0.529	In
Bottom	0.374	In	0.842	In
Top	18.1	Out	8.63	Out
Total Inflow	17.4		8.65	
Total Outflow	18.1		8.63	
Mass balance (In-Out)	−0.675		0.0255	

Figure 4-3. *Relative frequency histogram of $\log_{10}$ travel time for the Updated Base Case (50 realisations, each with 120 starting positions). Results for a flow porosity of $\varepsilon_f = 1x10^{-4}$.*
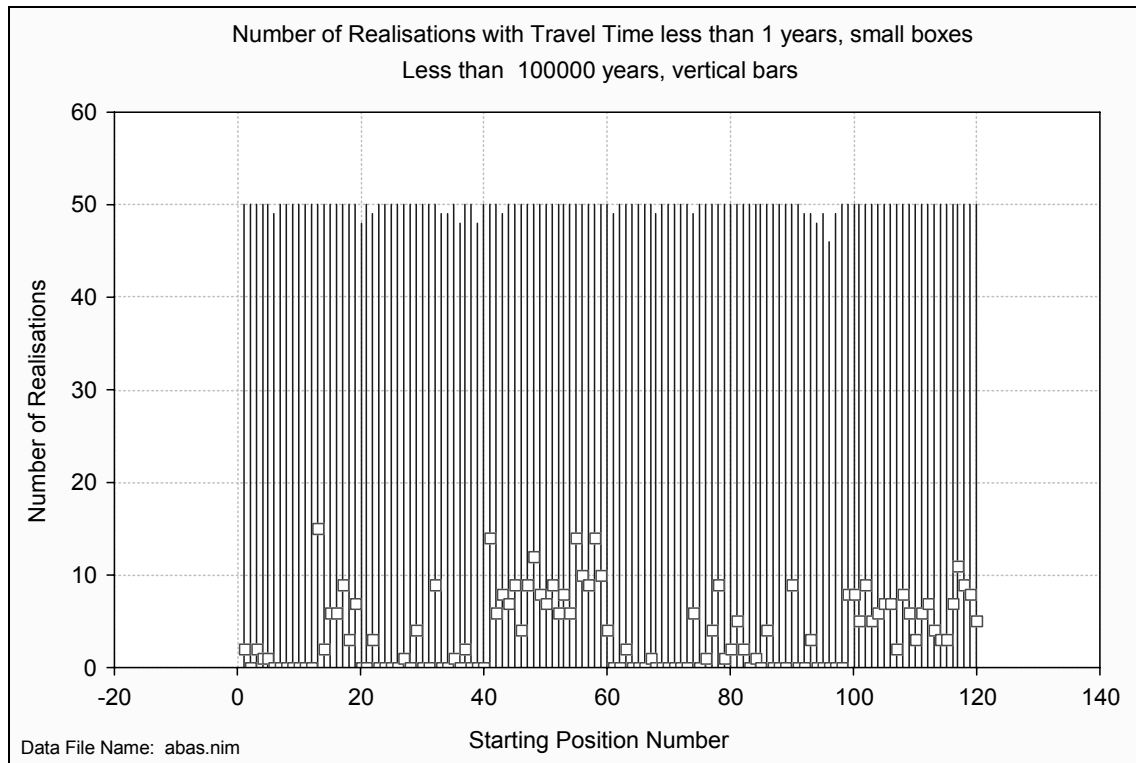
Figure 4-4. *Number of realisations with travel times less than 1 year (squares) and 100,000 years (lines), by stream tube number for Aberg Updated Base Case. Results for a flow porosity of $\varepsilon_f = 1x10^{-4}$.*

Figure 4-5 presents the histogram of $\log_{10}$ canister flux for the ensemble; it is unaffected by the maximum simulation time. Figure 4-6 is a plot of $\log_{10}$ travel time versus $\log_{10}$ canister flux, showing an inverse correlation (high canister flux is correlated with shorter travel times). The repeated travel-time values of 100,000 years represent pathlines that fail to exit at the top surface of the model. Analogous plots of $\log_{10}$ travel time versus $\log_{10}$ canister flux for the other upscaling methods are nearly identical, and are not included in this report.

Figure 4-7 is a map of exit locations; the parallel lines show the location of the hypothetical depositions tunnels projected to the upper surface. The exit locations are gathered near coastlines or in the water, where the upward gradient carries particles upward along the major fracture zones of the SCD to the Baltic Sea.
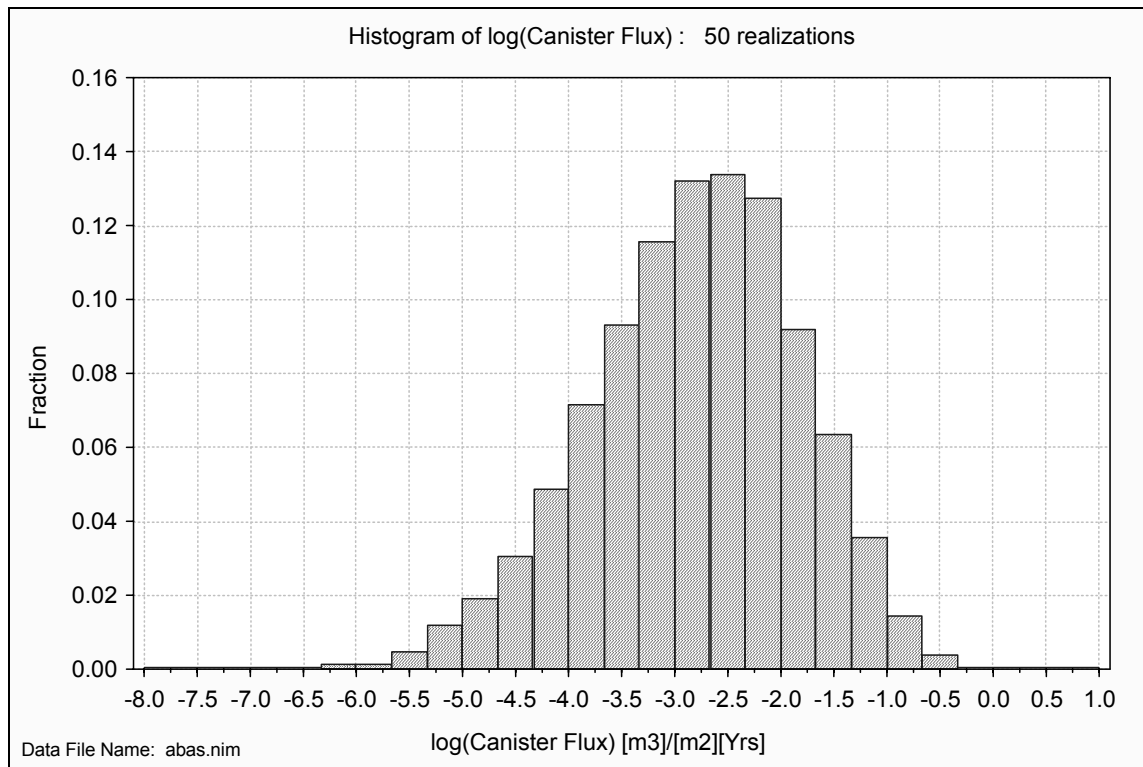

Figure 4-5. *Relative frequency histogram of $\log_{10}$ canister flux for Aberg Updated Base Case (50 realisations, each with 120 starting positions).*
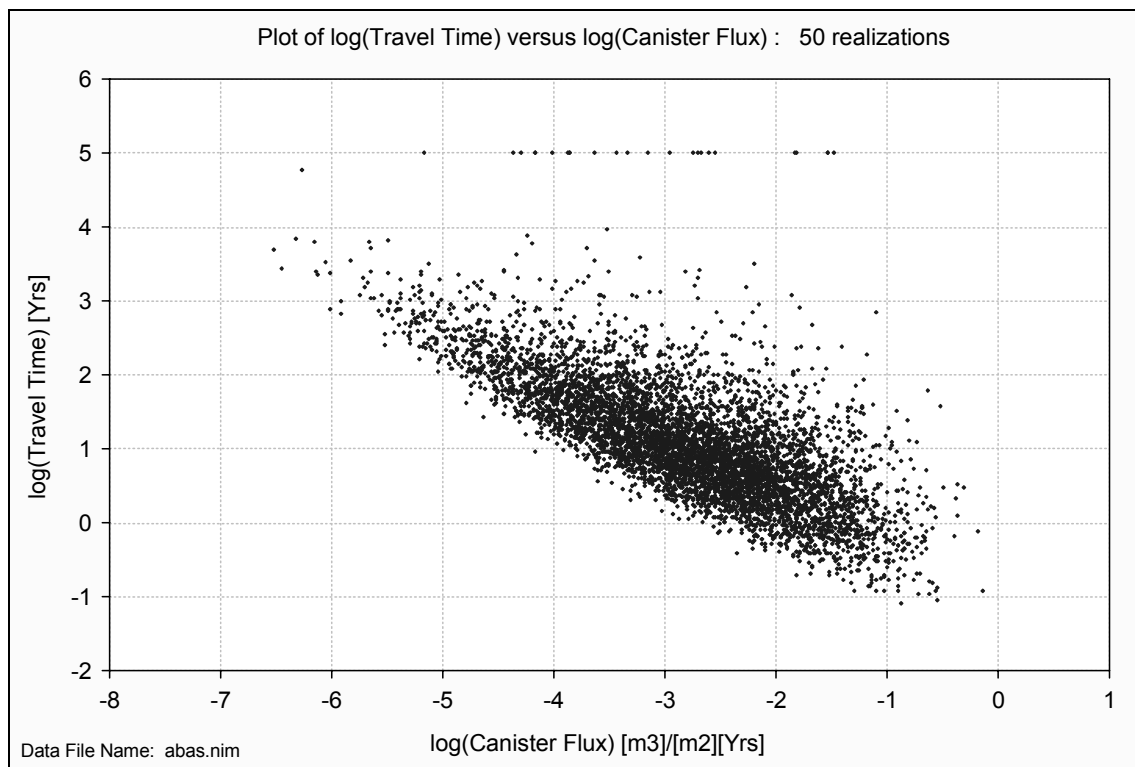
.

Figure 4-6. *Log$_{10}$ travel time versus log10 canister flux for Aberg Updated Base Case, 50 realisations each with 120 starting positions. Results for a flow porosity of $\varepsilon_f = 1x10^{-4}$.*
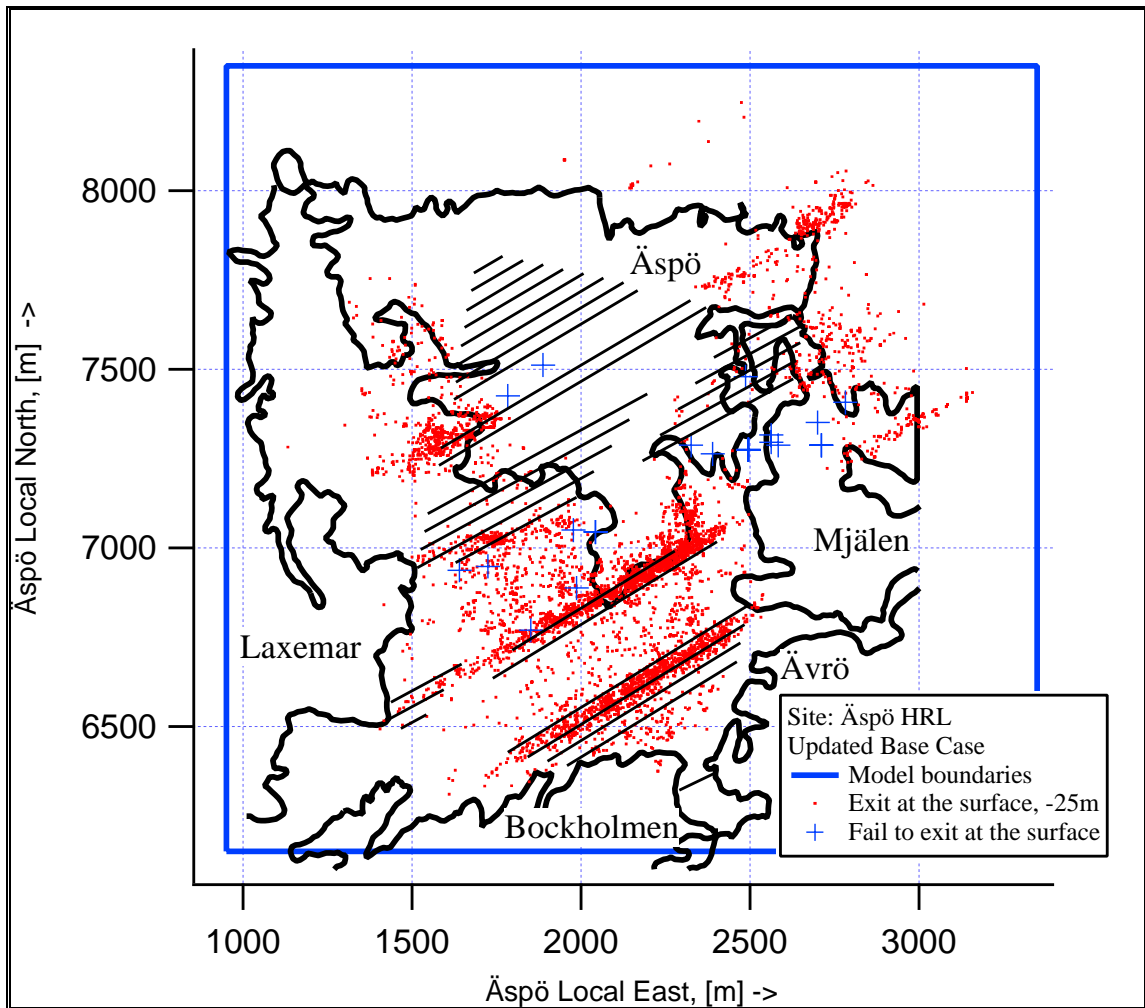
Figure 4-7. *Exit locations for 50 realisations of Aberg Updated Base Case.*

4.2 Alternative Method I

The first alternative approach to upscaling is a simple modification of the SR 97 approach: assume that the fracture zones of the SCD are two-dimensional features, and consequently increase the mean hydraulic conductivity of the fracture zones. Table 4-3 presents the summary statistics for this alternative, where approximately1.0 percent of the particles fail to exit at the upper boundary. For 50 realisations of this alternative, the median travel time is 8.85 years with a log-scale variance of 0.720; the median canister flux is 1.89×10^{-3} m/yr with a log-scale variance of 1.032; and the median F-quotient of 8.85×10^{5} yr/m with a log-scale variance of 0.720. Relative to the SR 97 approach, the medians of travel time and F-quotient are decreased, the median of canister flux is increased, and the variances of all performance measures have increased. The 5th percentile of travel time has decreased, suggesting that the increased hydraulic conductivities of the SCD have resulted in earlier first arrival times. Figures 4-8 and 4-9 show that the histograms of $\log_{10}$ travel time and $\log_{10}$ canister flux for Alternative

Method I are indistinguishable from those of the SR 97 method for upscaling. The exit locations within one realisation of this alternative show no obvious shift of particle exit locations relative to those of the SR 97 method for upscaling (Figure 4-10).

Table 4-3. Statistics for the Aberg Base Case using Alternative Method I. Statistics for t_w and F-quotient are calculated with only the path lines exiting at the upper boundary. A flow porosity of $\varepsilon_f = 10^{-4}$ and a flow-wetted surface of $a_r = 1.0$ m^{-1} are used to calculate t_w and the F-quotient.

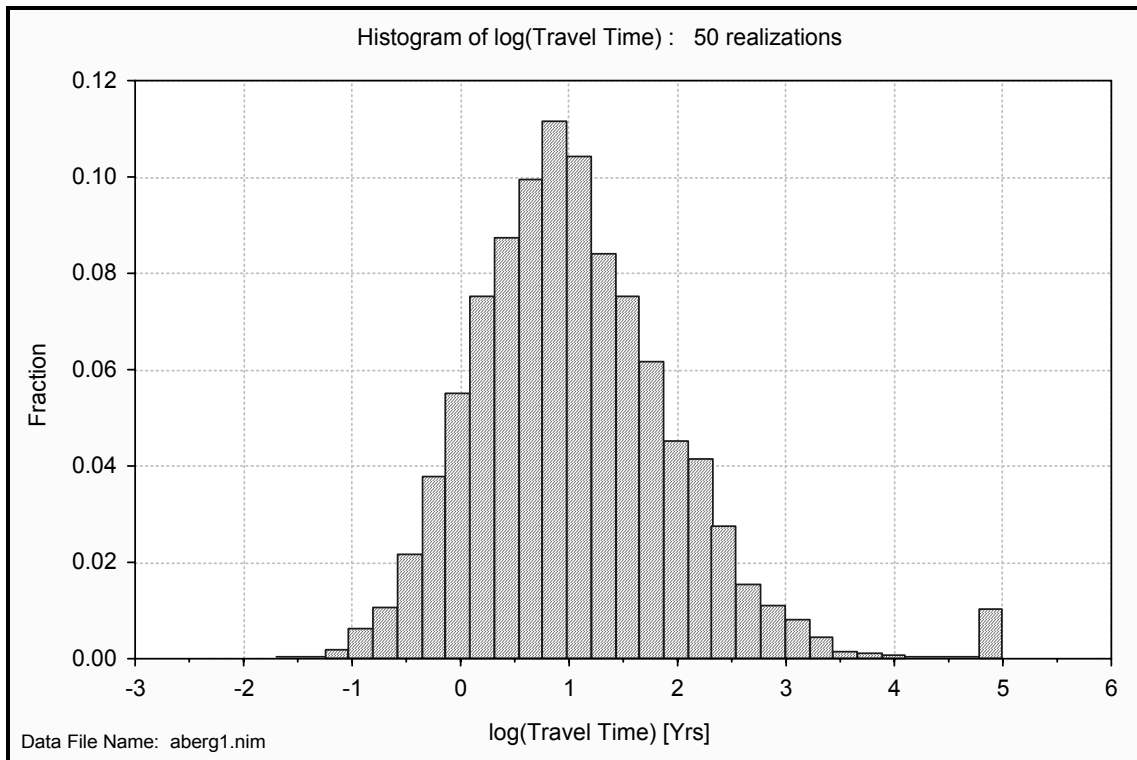|	Log$_{10}$ t_w	Log$_{10}$ q_c All	Log$_{10}$ q_c Exiting	Log$_{10}$ F-quotient
Mean	1.009	–2.777	–2.774	5.009
Median	**0.947**	**–2.723**	–2.718	**4.947**
Variance	**0.720**	**1.032**	1.036	**0.720**
5th percentile	–0.301	–4.563	–4.563	3.699
25th percentile	0.408	–3.433	–3.434	4.408
75th percentile	1.560	–2.060	–2.054	5.560
95th percentile	2.480	–1.209	–1.201	6.480

Figure 4-8. *Relative frequency histogram of log$_{10}$ travel time for Aberg Method I (50 realisations, each with 120 starting positions). Results for a flow porosity of $\varepsilon_f = 1x10^{-4}$.*
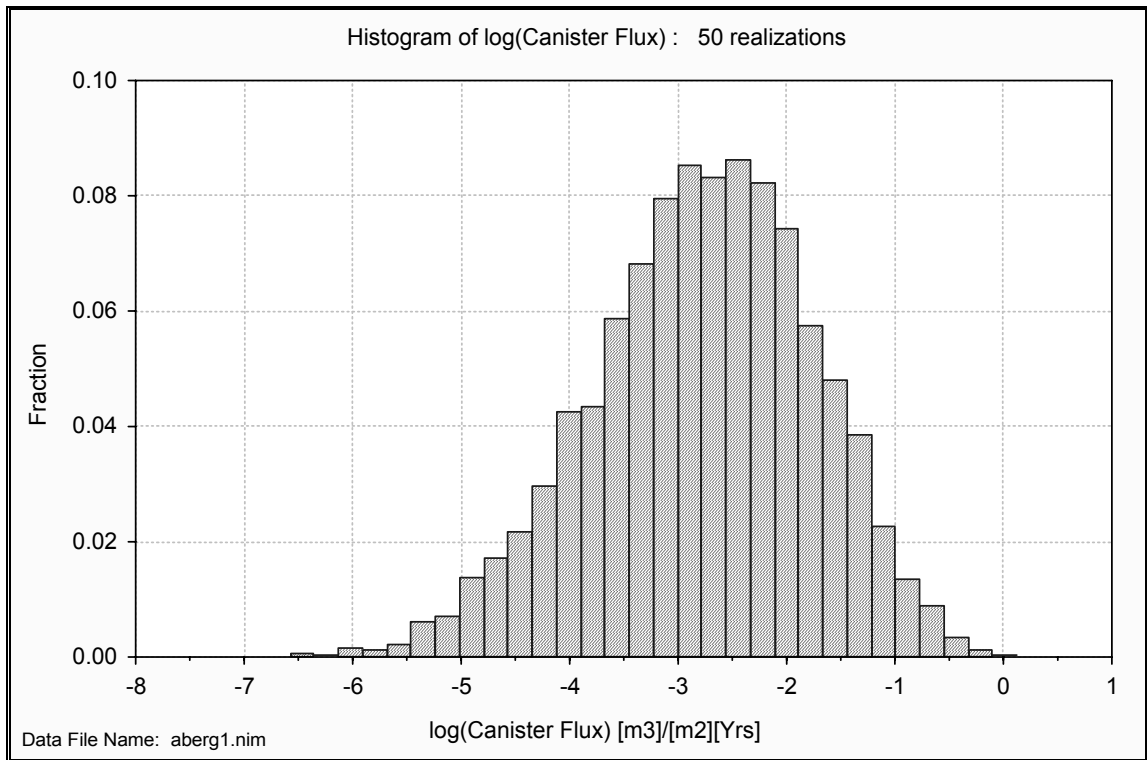
Figure 4-9. *Relative frequency histogram of log$_{10}$ canister flux for Aberg Method I (50 realisations, each with 120 starting positions).*
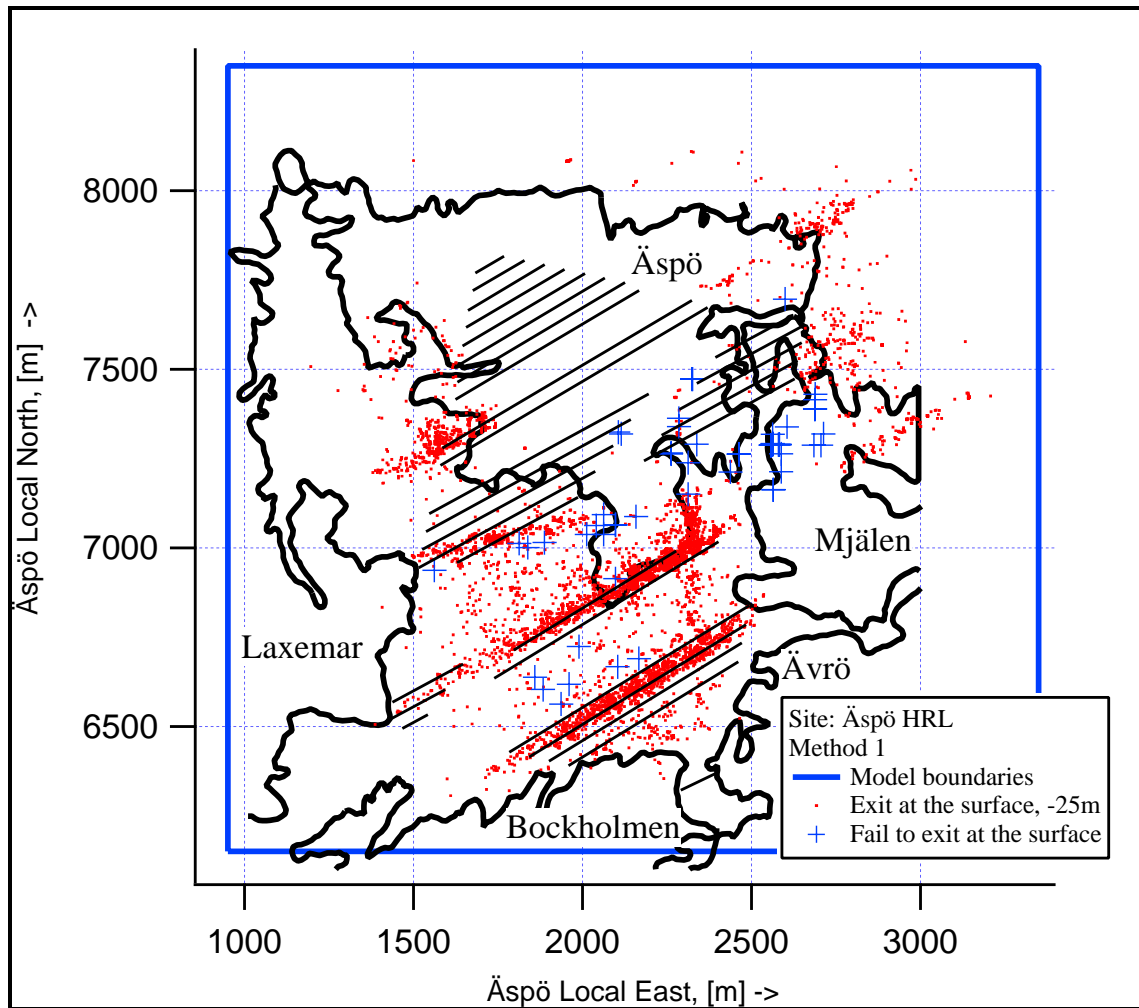
Figure 4-10. *Exit locations for 50 realisations of Method I.*

Table 4-4 presents the net flow over each boundary of the site-scale domain for Alternative Method I versus those of the regional model. As in the flow balance for the SR 97 approach to upscaling, the majority of groundwater flow enters from the west and exits out the upper surface to the Baltic Sea. The flow balance is improved relative to the SR 97 approach, with an error of approximately 10 to 15 percent (as a percentage of the total inflow or outflow). The flow across several of the surfaces of the domain is on the same order as the flow balance error of the regional model; this suggests that further refinement of upscaling will require a more accurate regional flow balance.

Table 4-4. Boundary flow consistency for Aberg using Alternative Method I, regional model versus site-scale model.

Model Surface	Net Flow Through Site Model Surfaces (m^3/s x 10^{-3})			
	Regional Model		Site-Scale Model Method I	
West	13.7	In	11.1	In
East	0.916	In	3.78	In
South	1.81	In	1.70	In
North	0.625	In	0.744	In
Bottom	0.374	In	1.82	In
Top	18.1	Out	19.2	Out
Total Inflow	17.4		19.2	
Total Outflow	18.1		19.2	
Mass balance (In-Out)	−0.675		0.0063	

4.3 Alternative Method II

The second alternative approach to upscaling uses the same two-dimensional assumption for the SCD as in Alternative I, but adapts stochastic continuum solutions for effective conductivity to upscale hydraulic conductivities of the SRD, and uses geostatistical regularisation to upscale the variogram. This dramatically reduces the variance of log_{10} hydraulic conductivity, and slightly increases the upscaled means of log_{10} hydraulic conductivity for the SRD. Although the upscaled means of the block hydraulic conductivities in the SRD have all slightly increased (Table 3-1), equation 3-4 implies that the dramatic reduction in the variance decreases the effective hydraulic conductivities for the SRD, and leaves the hydraulic conductivities for the SCD the same as in Alternative Method I. Table 4-5 presents the summary statistics for this alternative where approximately 0.1 percent of the particles fail to exit at the upper boundary. For 50 realisations of this alternative, the median travel time is 11.3 years with a log-scale variance of 0.501; the median canister flux is 1.32 x 10^{-3} m/yr with a log-scale variance of 0.602; and the median F-quotient of 1.13 x 10^5 yr/m with a log-scale variance of 0.501. Relative to the SR 97 method for upscaling, the medians of travel time and F-quotient are approximately the same, but the median of canister flux is slightly lower for Alternative Method II. The 5th percentile of travel time has become longer, suggesting that the decreased variance of log_{10} hydraulic conductivities has resulted in later first arrival times. The variances of the performance measures are decreased, attributed to the large reduction in the variance of hydraulic conductivity. These differences are believed to be larger than the statistical fluctuations of the Monte Carlo simulation as implied from differences discussed in Section 4.1

Figures 4-11 and 4-12 present histograms of log_{10} travel time and log_{10} canister flux for Alternative Method II, which are indistinguishable from those of the SR 97 and Method I. The exit locations within one realisation of this alternative are shifted relative to those of the previous upscaling approaches (compare Figures 4-7, 4-10, and 4-13). This can be partially explained by equation 3-3, which describes both the scale dependence of

Table 4-5. Statistics for the Aberg Base Case using Alternative Method II. Statistics for t_w and F-quotient are calculated with only the path lines exiting at the upper boundary. A flow porosity of $\varepsilon_f = 10^{-4}$ and a flow-wetted surface of $a_r = 1.0$ m^{-1} are used to calculate t_w and the F-quotient.

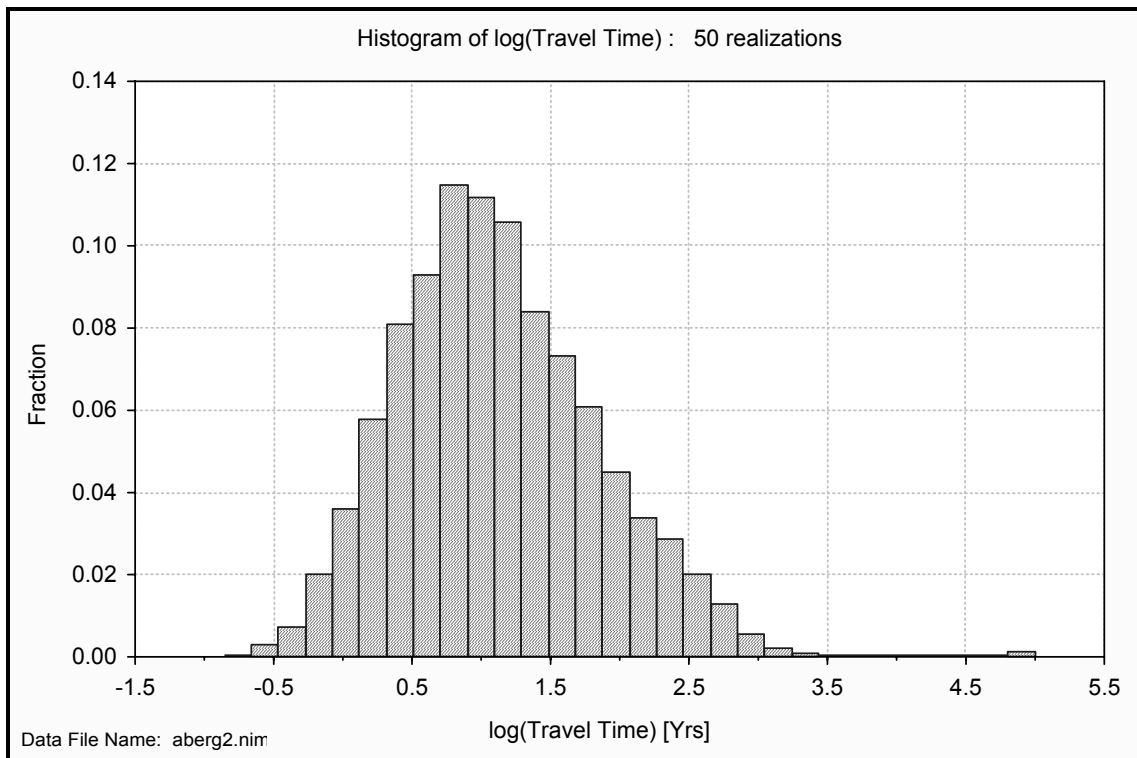|	$\mathbf{Log_{10}\ t_w}$	$\mathbf{Log_{10}\ q_c}$ All	$\mathbf{Log_{10}\ q_c}$ Exiting	$\mathbf{Log_{10}}$ F-quotient
Mean	1.114	–2.914	–2.914	5.114
Median	**1.054**	**–2.88**	–2.88	**5.054**
Variance	**0.501**	**0.602**	0.602	**0.501**
5th percentile	0.037	–4.251	–4.251	4.037
25th percentile	0.607	–3.442	–3.442	4.607
75th percentile	1.577	–2.365	–2.365	5.577
95th percentile	2.405	–1.704	–1.703	6.405

Figure 4-11. *Relative frequency histogram of log$_{10}$ travel time for Aberg Method II (50 realisations, each with 120 starting positions). Results for a flow porosity of $\varepsilon_f = 1x10^{-4}$.*

three-dimensional media and the scale independence of two-dimensional media. The consequence is that the reduced variance of $\log_{10}$ hydraulic conductivity decreases the effective conductivity of the SRD but has little impact on the effective conductivity of the SCD. This increases the contrast between the conductor and the rock domains, and makes the fracture zones the dominant water-conducting features of the model.
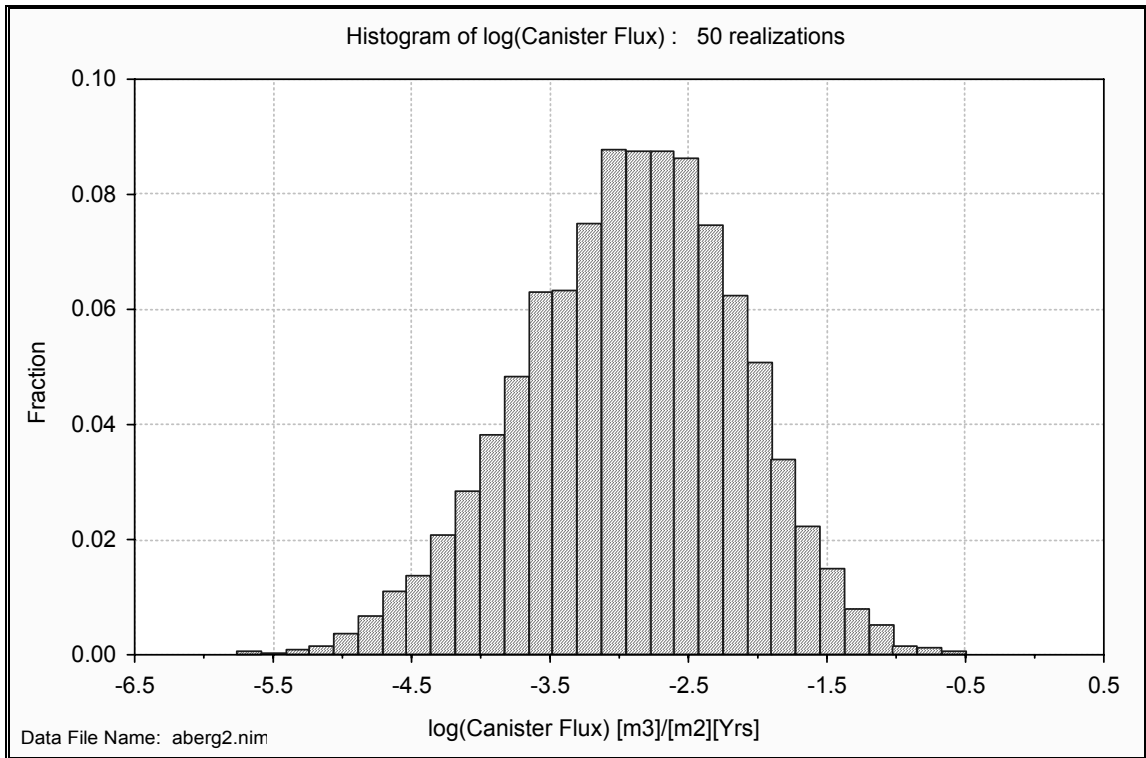

Figure 4-12. *Relative frequency histogram of $\log_{10}$ canister flux for Aberg Method II (50 realisations, each with 120 starting positions).*
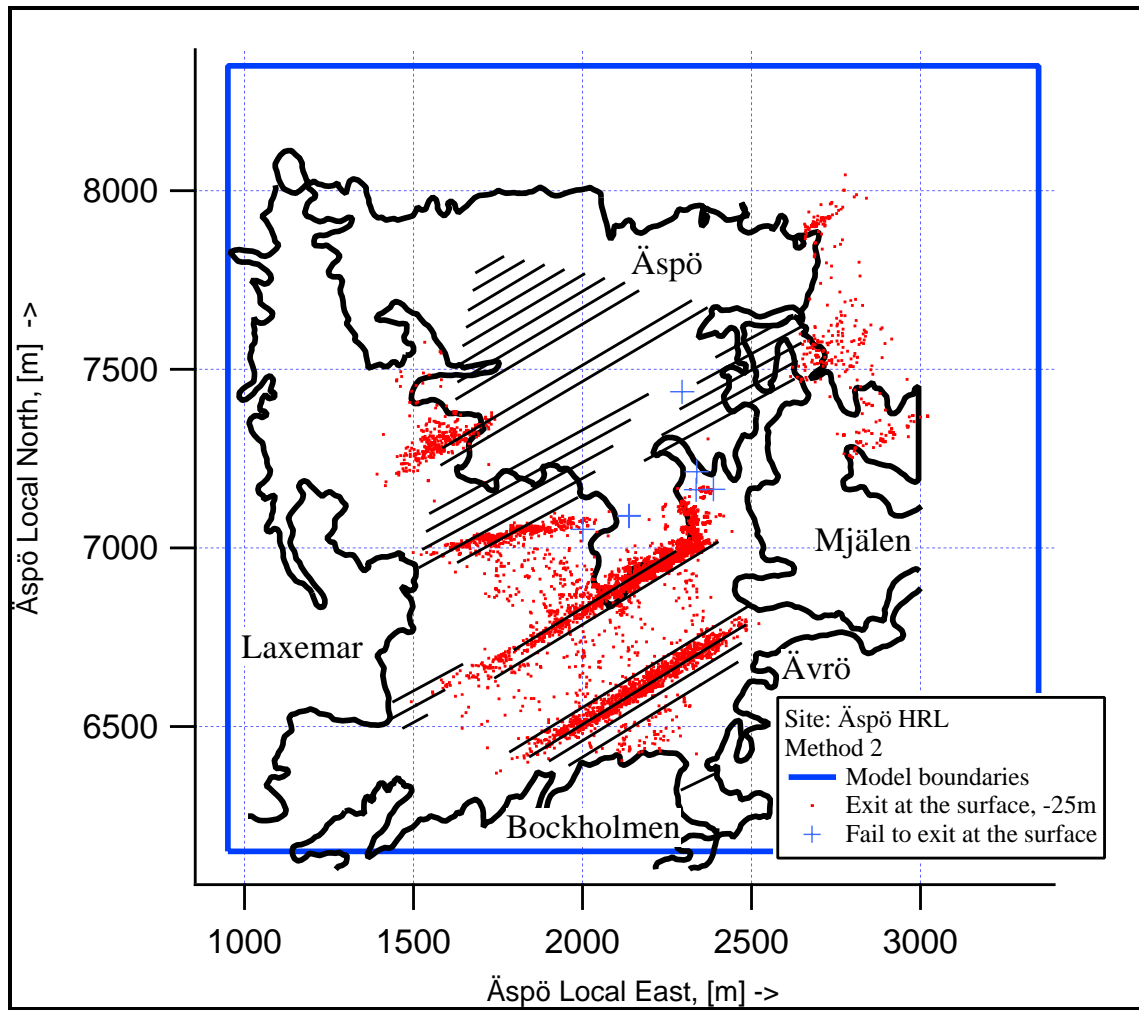
Figure 4-13. *Exit locations for 50 realisations of Alternative Method II.*

Table 4-6 presents the net flow over each boundary of the site-scale domain for Alternative Method II versus those of the regional model. As in the flow balance for the SR 97 approach to upscaling, the majority of groundwater flow enters from the west and exits out the upper surface to the Baltic Sea. The boundary flows of the site model using Alternative Method II are approximately ¼ to 1/3 the boundary flows of the regional model.

Table 4-6. Boundary flow consistency for Aberg using Alternative Method II, regional model versus site-scale model.

Model Surface	Net Flow Through Site Model Surfaces (m^3/s x 10^{-3})			
	Regional Model		Site-Scale Model Method II	
West	13.7	In	3.57	In
East	0.916	In	0.0174	In
South	1.81	In	1.03	In
North	0.625	In	0.142	In
Bottom	0.374	In	0.940	In
Top	18.1	Out	5.74	Out
Total Inflow	17.4		5.70	
Total Outflow	18.1		5.73	
Mass balance (In-Out)	−0.675		0.0326	

5   Summary and discussion

This study has evaluated the uncertainties of upscaling of hydraulic conductivity for their impact on groundwater flow models in the context of performance assessments for the disposal of nuclear waste. We have considered four upscaling approaches, each designed to determine the means and variogram of the distribution of $\log_{10}$ hydraulic conductivities for the numerical blocks of a finite difference model. The four approaches are:

1)   The Base Case: as in SR 97, empirically upscaling the mean conductivity via the observed scale dependence of measurements, and adjusting the variogram via numerical regularisation based on Moye's formula;

2)   Alternative Method I: empirically upscaling and Moye-based regularisation as in SR 97, but considering fracture zones as two-dimensional features;

3)   Alternative Method II: adapting analytical solutions for the effective conductivity to upscale the mean, and geostatistical regularisation for variogram; and

4)   Alternative Method III: the analytical approach of /Indelman and Dagan, 1993b/.

The Base Case consisted of two simulations, one to evaluate changes in the computational details (the Rerun) and another to evaluate the effects of updating the properties of two minor fracture zones (the Update). The four approaches were applied to the groundwater flow models of Aberg, one of the hypothetical repositories examined in SR 97. The methods have been evaluated for their affects on simple measures of repository performance and for the consistency of boundary flows between the nested models. The performance measures included the canister flux, the advective travel time from representative canister locations to the ground surface, and the F-quotient. These performance measures were compiled over a set of 50 Monte Carlo simulations of 120 particle tracking starting positions as representative disposal canister positions. The results of the simulations are summarised by their respective boundary flows (Table 5-1) and the statistics of their performance measures (Table 5-2).

5.1   The SR 97 Base Case and computational stability

The Aberg Base Case as presented in this study differs slightly from that presented by /Walker and Gylling, 1998/ for the Aberg Base Case in SR 97. These differences are minor changes in the computational details and the update of the effective hydraulic conductivities for two minor fracture zones. Two Monte Carlo simulations evaluated the effects of these changes so that they could be isolated from the effects of changing the upscaling methods. The effects of the computational changes and updates on the results are small, as evidenced by the small changes in the boundary flows and summary statistics of the simplified performance measures (Tables 5-1 and 5-2). These results suggest that the differences arising from computational changes and updates to the

properties of minor zones are within the statistical fluctuations of the Monte Carlo estimates. This in turn suggests that the SR 97 results for this site are robust with respect to minor variations in computations and parameters. This study uses the updated Aberg Base Case, also known as 'the Update', as the reference case for the SR 97 approach to upscaling in the remainder of this summary and discussion.

Table 5-1. Boundary Flux Consistency for the Aberg Regional Model versus the SR 97 Base Case, the Updated SR 97 Base Case, and the Alternative Upscaling methods. The SR 97 Base Case boundary flows were calculated using five realisations; all other site-scale models used 50 realisations.

| Model Surface | Regional Model | Net Flux Through Subdomain (m^3/s x 10^{-3}) | | | |
| | | SR 97 upscaling approach | | Alternative upscaling approaches | |
		SR 97 Base Case	Update	Method I	Method II
West (in)	13.7	4.92	5.43	11.1	3.57
East (in)	0.916	0.77	1.15	3.78	0.0174
South (in)	1.81	0.846	0.698	1.70	1.03
North (in)	0.625	0.538	0.529	0.744	0.142
Bottom (in)	0.374	1.03	0.842	1.82	0.940
Top (out)	18.1	8.11	8.63	19.2	5.74
Total Inflow	17.4	8.11	8.65	19.2	5.70
Total Outflow	18.1	8.11	8.63	19.2	5.73
Mass balance (In-Out)	−0.675	−0.0037	0.0255	0.0063	0.0326

Table 5-2. Summary of study results for performance measure statistics.

Performance Measure		SR 97 Base Case	SR 97 Base Case Update	Method I	Method II
Log$_{10}$ Travel time (years)	Median	1.015	1.028	0.947	1.054
	Variance	0.599	0.613	0.720	0.501
	5th percentile	–0.125	–0.131	–0.301	0.037
Log$_{10}$ Canister Flux (m/y)	Median	–2.736	–2.744	–2.723	–2.88
	Variance	0.935	0.946	1.032	0.602
F-quotient (y/m)	Median	5.015	5.028	4.947	5.054
	Variance	0.599	0.613	0.720	0.501

5.2   Comparison

Relative to the SR 97 approach to upscaling, the three alternative methods of upscaling increase the mean log$_{10}$ hydraulic conductivity of blocks within the fracture zones of the SCD; the values are effectively equal to those of the Regional model. Alternative Methods II and III employ geostatistical regularisation of the variogram, which decreases the variance of log$_{10}$ hydraulic conductivity dramatically relative to that of SR 97 and Alternative Method I. Alternative Method III results in a parameter set that is very similar to that of Method II, and is therefore not carried forward to Monte Carlo simulation.

The boundary flows of Alternative Method I are approximately equal to the boundary flows of the regional model, with an error of 10 to 15 percent (as a percentage of the total inflow or outflow), comparable to errors reported for nested deterministic models /Leake et al, 1998/. As seen in Table 5-1, a boundary-by-boundary comparison is less satisfactory, but for some model surfaces the differences are no greater than the error in the regional mass balance (–0.675 x 10^{-3} m^3/s). Table 5-2 shows that, in comparison to the SR 97 approach, the median travel time is shortened from 10.7 years to 8.85 years, a difference that is larger than the statistical fluctuation of the simulations. The median canister flux is increased from 1.80 x 10^{-3} m/yr to 1.89 x 10^{-3} m/yr, a difference that is approximately the same as the statistical fluctuation of the Monte Carlo simulations. The variances of all performance measures are increased, and this increase is several

times larger than the changes seen in the analysis of the sensitivity to computational changes. The 5th percentile of travel time has decreased, suggesting that the increased hydraulic conductivity of the SCD has resulted in earlier first arrival times.

Table 5-1 also shows that the boundary flows of Alternative Method II are approximately 1/3 to 1/4 those of the regional model, although the orientations are the same for both models. In comparison to the SR 97 approach, the median of the travel time is increased from 10.7 years to 11.3 years, a difference that is approximately the same as the statistical fluctuation of the simulations. The median of the canister flux is decreased from 1.80 x 10^{-3} m/yr to 1.32 x 10^{-3} m/yr, a difference that is larger than the statistical fluctuation of the simulations. The variances of all performance measures are decreased, and this decrease is several times larger than the changes seen in the analysis of the sensitivity to computational changes. The 5th percentile of travel time of this method has become longer than that of the SR 97 approach, suggesting that the decreased variance of $\log_{10}$ hydraulic conductivities has resulted in later first arrival times. The results of Alternative Method II suggests that the change in variance decreases the effective conductivity of the SRD, and that flow through the SRD is as important to the flow balance as is the flow in the SCD. It is also possible that the variance of $\log_{10}$ conductivity impacts the flow in the SCD, indicating that SCD are not strictly two-dimensional stochastic continua.

5.3   Conclusions

The comparison of alternative approaches to upscaling indicates that, for the methods examined in this study, Alternative Method I results in the greatest consistency of boundary flows between the regional and site-scale models. This method uses the scale dependence of hydraulic conductivity observed at Äspö for upscaling in the rock domains, the hydraulic conductivities of the large-scale interference tests for the conductor domain, and a numerical regularisation based on Moye's formula for the variogram. The assumption that the fracture zones of the SCD behave as two-dimensional media results in the greatest change to the median of travel time, and improves the agreement between the boundary flows of the regional and site-scale models. The improvement in the flow balance suggests that upscaling algorithms should be tailored to the dimensionality of the hydraulic units. In the case of site-scale models of groundwater flow in fractured rocks, this will commonly mean that fracture zones will use two-dimensional scaling algorithms, and the rock mass will use three-dimensional scaling algorithms.

The uncertainty of methods for upscaling hydraulic conductivity appears to have several impacts on the performance measures. The greatest impacts of this uncertainty appear to be on the variances of the performance measures and on the earliest arrival times of particles released from representative canister positions. The upscaling of the variogram of $\log_{10}$ hydraulic conductivity has a direct impact on the canister flux variability: the greater the variance of $\log_{10}$ hydraulic conductivity, the greater the variances of the canister flux. The uncertainty of methods for upscaling hydraulic conductivity appears to have a relatively small impact on medians of the performance measures.

Another impact of the uncertainty in upscaling is attributed to the effective conductivity of the SRD: a large hydraulic conductivity variance makes the effective conductivity of a three-dimensional medium much larger than the its mean conductivity. For the SR 97 model of Aberg, the variance is large enough that the effective conductivity of the SRD is large enough that changes in the variance changes the overall flow balance of the model. Thus, the SRDs are effectively as important as the SCD to the flow balance of the Aberg model.

The above conclusions regarding upscaling approaches have several implications for other applications of HYDRASTAR. Alternative Method I (observed scale dependence, treating the fracture zones as two-dimensional features, and Moye-based regularisation) appears to be the best choice for this application, but many sites will not have data sufficient to infer the scale dependence of hydraulic conductivity. An alternative might be to use HYDRASTAR's built-in Moye-based upscaling algorithm for both the block-scale means and variogram. However, the results of this study also imply that upscaling algorithms should be tailored to the dimensionality of separate domains, and the current version of HYDRSATAR includes a single upscaling algorithm. Thus, in the case of limited site-scale data, the only viable approach appears to be to calibrate the block-scale conductivities to such flow and head data that are available. In any case, the uncertainty of the inferred parameters and upscaling should still be evaluated using alternative-scenario calculations, as were conducted in SR 97.

The errors in regional versus site-scale boundary flows might be interpreted to mean that the nested approach should be abandoned, but scale effects might still be difficult to avoid. For example, rather than a nested approach, one alternative would be to use a single model of regional extent and a highly detailed subregion to represent the site-scale domain. Another approach would be to use the dual-grid method, where a detailed, site-scale domain is solved separately but is numerically coupled to the regional model. Although either approach rigorously maintains continuity across the site-scale boundary and thus eliminates the question of flow balance, including additional detail in a subregion of a model can change the local variance of hydraulic conductivity. Just as in a nested model, this can result in the subregion having an anomalously different effective conductivity in the area of interest. Such a change in effective conductivities should also be expected to affect deterministic models that include a small region with increased degree of heterogeneity /Leake and Claar, 1999/.

Overall, the uncertainty associated with the upscaling of hydraulic conductivity appears to have a small impact on the medians of the performance measures, a noticeable impact on the variances and the early arrival times, and an important impact on the flow balance between nested models. The flow balance and the variances of the performance measures are apparently sensitive to the total variance and the nugget variance of $\log_{10}$ hydraulic conductivity. This indicates that measurement and inference of the parameters of the variogram is as important to performance assessment as the inference of the expected values of $\log_{10}$ hydraulic conductivity. This apparent sensitivity also indicates that the upscaling of the variogram is also important to performance assessment. However, while the impacts of this uncertainty are larger than the statistical fluctuation of the Monte Carlo simulations, such variability would be overwhelmed by other uncertainties in the performance assessment of a repository for nuclear waste disposal.

Acknowledgements

References

Andersson J, Hermanson J, Elert M, Gylling B, Moreno L and Selroos J-O, 1998. Derivation and treatment of the flow wetted surface and other geosphere parameters in the transport models FARF31 and COMP23 for use in safety assessment, SKB Report R-98-60, Swedish Nuclear Fuel and Waste Management Co, Stockholm, Sweden.

Dagan G, 1989. Flow and Trnasport in Porous Formations. Springer-Verlag, 465 pp.

Dagan G, 1993. High-order correction of effective permeability of heterogeneous isotropic formations of lognormal conductivity distributions. Transport in Porous Media, 12, p 279–290.

Dverstorp B, Geier J and Voss C, 1996. SITE-94. Simple Evaluation of Groundwater Flow and Radionuclide Transport at Äspö. Swedish Nuclear Power Inspectorate, SKI Report 96:14, Stockholm, Sweden.

Gelhar L W and Axness C L, 1983. Three-dimensional stochastic analysis of macrodispersion in aquifers. Water Resources Research 19 (1): 161–180.

Gelhar L W, 1993. Stochastic subsurface hydrology. Prentice Hall, New Jersey.

Gutjhar A L, Gelhar L W, Bakr A A and MacMillan J R, 1978. Stochastic analysis of spatial variability in subsurface flows: 2. Evaluation and application. Water Resources Research 14 (5): 953–959.

Gylling B and Eriksson L, 2001. Assessment model validity document – HYDRASTAR: A stochastic continuum program for groundwater flow. Swedish Nuclear Fuel and Waste Management Co, SKB Report R-01-61, Stockholm, Sweden.

Holmén J G, 1997. On the Flow of Groundwater in Closed Tunnels: Generic Hydrogeologic Modelling of Nuclear Waste Repository SFL 3-5, Ph.D. thesis, Inst. of Earth Sciences, Uppsala University, Uppsala, Sweden, 286 pp.

Indelman P, 1993. Upscaling of permeability of anisotropic heterogeneous formations 3. Applications. Water Resources Research, 29(4), p 935–943.

Indelman P and Dagan G, 1993a. Upscaling of permeability of anisotropic heterogeneous formations 1. The general framework. Water Resources Research, 29(4), p 917–923.

Indelman P and Dagan G, 1993b. Upscaling of permeability of anisotropic heterogeneous formations 2. General structure and small perturbation analysis. Water Resources Research, 29(4), p 925–933.

Indelman P and Dagan G, 1993c. Upscaling of conductivity of heterogeneous formations: General approach and application to isotropic media, Transport in Porous Media, 12, p 161–183.

Jackson C P, Hoch A R and Todman S, 2000. Self-consistency of a heterogeneous continuum porous medium representation of a fractured medium, Water Resources Res. 36:1, p189–202.

Journel A G and Huijbregts C J, 1978. "Mining geostatistics." Academic Press, London, 600 pp.

KBS, 1983. Final storage of spent nuclear fuel – KBS-3, SKBF/KBS, Stockholm, Sweden (5 volumes).

LaPointe P R, 1994. Evaluation of stationary and non-stationary geostatistical models for inferring hydraulic conductivity values at Äspö. Swedish Nuclear Fuel Management Co, SKB Technical Report TR 94-22, Stockholm, Sweden.

Leake S A, Lawson P W, Lilly M R and Claar D V, 1998. Assignment of boundary conditions in embedded groundwater flow models, Ground Water 36 (4), p 621–625.

Leake S A and Claar D V, 1999. Procedures and Computer Programs for Telescopic Mesh Refinement Using MODFLOW, USGS Open-File report 99-238, 53 pp.

Matheron G, 1967. Elements pour une theorie pour des milieux poreux, Masson et Cie, Paris.

McKenna S A and Rautman C A, 1996. Scaling of material properties for Yucca Mountain: Literature review and numerical experiments on saturated hydraulic conductivity, Sandia National Laboratory Report SAND95-2338, Albuquerque, NM.

Moye D G, 1967. Diamond drilling for foundation exploration, Civil Engineering Trans. Austrailia, p 95–100.

Munier R, Sandstedt H and Niland L, 1997. Förslag till principiella utformningar av förvar enligt KBS-3 för Aberg, Beberg och Ceberg, SKB Report R 97-09, Swedish Nuclear Fuel and Waste Management Co, Stockholm, Sweden.

NEA, 1991. Review of safety assessment methods, Nuclear Energy Agency, Paris, France.

Neuman S and Jacobsen E, 1984. Analysis of nonintrinsic spatial variability by residual kriging with application to regional groundwater levels. Mathematical Geology, 16(5), p 499–521.

Neuman S, 1988. A proposed conceptual framework and methodology for investigating flow and transport in Swedish crystalline rocks, SKB Working Report AR 88-37, Swedish Nuclear Fuel and Waste Management Co, Stockholm, Sweden.

Niemi A, 1995. Modelling of Äspö hydraulic conductivity data at different scales by means of 3-dimensional Monte Carlo simulations. Swedish Nuclear Fuel Management Co, SKB International Corporate Report ICR 95-08, Stockholm, Sweden.

Norman S, 1992. HYDRASTAR – A code for stochastic simulation of groundwater flow, SKB Technical Report TR 92-12, Swedish Nuclear Fuel and Waste Management Co, Stockholm, Sweden.

Pozdniakov S P and Tsang C F, 1999. A semianalytical approach to spatial averaging of hydraulic conductivity in heterogeneous aquifers, J. Hydrology 216, p 78–98.

Renard P H and de Marsily G, 1997. Calculating equivalent permeability: A review. Advances in Water Resources, 20 (5,6), p 253–278.

Rhén I, Gustafson G, Stanfors R and Wikberg P, 1997. Äspö Hard Rock Laboratory – Geoscientific Evaluation 1997/5. Models based on site characterization 1986–1995. Swedish Nuclear Fuel and Waste Management Co, SKB Technical Report TR 97-06, Stockholm, Sweden.

Ritzi R W, Dominic D F, Slesers A J, Greer C B, Reboult E C, Telford J.A, Masters R W, Klohe C A, Bogle J L and Means B P, 2000. Comparing statistical models of physical heterogeneity in buried-valley aquifers, Water Resources Res. 36:11, p 3179–3192.

Rubin Y and Gómez-Hernández J J, 1990. A stochastic approach to the problem of upscaling of conductivity in disordered media: Theory and unconditional numerical simulations. Water Resources Research, 26(4), p 691–701.

Selroos J-O, Walker D D, Ström A, Gylling B and Follin S, 2002. Comparison of alternative modelling approaches for flow and transport in fractured rock, J. Hydrology, 257, p 174–188.

SKB, 1992. SKB 91: Final disposal of spent nuclear fuel. Importance of bedrock for safety, SKB Technical Report TR 92-20, Swedish Nuclear Fuel and Waste Management Co, Stockholm, Sweden.

SKB, 1999. Deep repository for spent nuclear fuel. SR 97 – Post-closure safety: Main report (Vol I, Vol II and Summary), Swedish Nuclear Fuel Management Co, SKB Technical Report TR-99-06, Stockholm, Sweden.

SKI, 1997. SKI Site-94 Deep repository performance assessment project. Swedish Nuclear Power Inspectorate, SKI Report 97:5, Stockholm, Sweden.

Svensson U, 1997. A regional analysis of groundwater flow and salinity distribution in the Äspö area, SKB Technical Report TR 97-09, Swedish Nuclear Fuel and Waste Management Co, Stockholm, Sweden.

Walker D, Rhén I and Gurban I, 1997. Summary of Hydrogeologic Conditions at Aberg, Beberg and Ceberg. Swedish Nuclear Fuel and Waste Management Co, SKB Technical Report 97-23, Stockholm, Sweden.

Walker D and Gylling B, 1998. Site-scale groundwater flow modelling of Aberg. Swedish Nuclear Fuel and Waste Management Co, SKB Technical Report TR 98-23, Stockholm, Sweden.

Walker D, Gylling B, Ström A and Selroos J-O, 2001. Hydrogeologic studies for nuclear waste disposal in Sweden, Hydrogeology Journal, vol 9, no 5, p 419–431.

Ward D, Buss D, Mercer J and Hughes S, 1987. Evaluation of a groundwater corrective action at the Chem-Dyne hazardous waste site using a telescopic mesh refinement modelling approach. Water Resources Research, 23(4): 603–617.

Wen X-H and Gómez-Hernández J J, 1996. Upscaling hydraulic conductivities in heterogeneous media: An overview. J. of Hydrology 183.

Winberg A, 1994. Geostatistical analysis of transmissivity data from fracture zones at Äspö, Swedish Nuclear Fuel Management Co, SKB Progress Report PR 25-94-17, Stockholm, Sweden.

Variogram regularisation

Introduction

Regularisation is a procedure used in mining geostatistics to determine the averaging effects that occur when sampling a spatially correlated random variable over a volume. It is relevant to this study because Alternative Methods II and III require the block average variogram, $\bar{\gamma}(v,v)$, and the regularised variogram, $\gamma_v(h)$, for their upscaling calculations. This appendix summarises the regularisation algorithms used in this study, which are a straightforward implementation of the algorithms presented in /Journel and Huijbregts, 1978/. Elementary algorithms for computing $\bar{\gamma}(v,v)$ are presented in /Journel and Huijbregts, 1978/ as FORTRAN subroutines GBAR and F. For the purposes of this study, these were modified slightly to permit computing $\gamma_v(h)$ and to use an input format compatible with GSLIB v2.0. We also derive several important properties of the regularised variogram.

Regularisation

Consider the semi-variogram as *γ(h)* of a point process, which may be the linear combination of models, i.e.,

$$\gamma(h) = C_0 + \gamma_1(h) \tag{A-1}$$

where C_0 is the nugget variance and *γ₁(h)* is a continuous function that describes the correlation between values of the point process separated by *h*, the lag spacing. Note that, for 2nd order stationary fields, $\sigma^2 = C_0 + \gamma_1(\infty)$. The regularisation (average value) of *γ(h)* over a support (sample) volume *v* is denoted $\gamma_v(h)$, and is defined by /Journel and Huijbregts, 1978, II.41/ as:

$$\gamma_v(h) = \bar{\gamma}(v, v_h) - \bar{\gamma}(v, v) \tag{A-2}$$

where

$$\bar{\gamma}(v,v) = \frac{1}{vv} \iint_{v\ v} \gamma(x - x')\ dx dx' \tag{A-3}$$

where *x* and x' are vectors that describe all points in *v,* and

$$\bar{\gamma}(v,v_h) = \frac{1}{vv_h} \int\limits_{v} \int\limits_{v_h} \gamma(u - u') \; dudu' \tag{A-4}$$

where u and u' are vectors with one end describing v and the other describing v_h. That is, $\bar{\gamma}(v,v)$ is the average of the point variogram within the volume v, while $\bar{\gamma}(v,v_h)$ is the average of the point variogram over volume v and a second volume v translated by h.

Some bounding values of the regularised semivariogram should be noted. If h is much larger than the dimensions of v, then the regularised semivariogram of equation A-2 can be approximated by:

$$\gamma_v(h) \cong \gamma(h) - \bar{\gamma}(v,v) \tag{A-5}$$

and as $h \to \infty$ for finite v, then $\sigma_v^2 = \gamma(\infty) - \bar{\gamma}(v,v)$. When the domains v and v_h coincide (h=0), then $\bar{\gamma}(v,v_h) \equiv \bar{\gamma}(v,v)$; thus by equation A-2, $\gamma_v(0) = 0$, regardless of C_0. When $C_0 \neq 0$, it should be noted that:

$$\bar{\gamma}(v,v) = \frac{1}{vv} \int\limits_{v} \int\limits_{v} \left[C_0 + \gamma_1(x - x') \right] dxdx' = C_0 + \bar{\gamma}_1(v,v) \tag{A-6}$$

and similarly for $\bar{\gamma}(v,v_h)$, so that in general $\bar{\gamma}_v(h) = \bar{\gamma}_1(v,v_h) - \bar{\gamma}_1(v,v)$, i.e., regularisation destroys the nugget variance, so that a regularised variogram never includes a nugget /Dagan, 1989/. Other limiting values may also be noted:

As $v \to 0$, $\quad \bar{\gamma}(v,v) \to 0$ so that $\bar{\gamma}_v(h) \to \gamma(h)$ $\tag{A-7}$

As $v \to \infty$, $\bar{\gamma}(v,v_h) \to \gamma(\infty)$,

so that $\bar{\gamma}(v,v) \to \gamma(\infty)$, $\bar{\gamma}_v(h) \to 0$, and $\sigma_v^2 \to 0$ $\tag{A-8}$

Numerical approximation

The integrations of equations A-3 and A-4 generally do not have closed-form solutions, and must be approximated numerically. /Journel and Huijbregts, 1978/ provide two algorithms for these approximations. The first approximates the nested integrations of equations A-3 and A-4 via a simple discretisation of the two volumes into a uniform grid, then summing the values of the process at each location. That algorithm, named GBAR, can be used for domains of different geometries and thus is quite versatile. However, it uses a relatively small number of points, and this is known to limit the accuracy of discrete algorithms when the integrand is rapidly changing. /Journel and Huijbregts, 1978/ presented a second algorithm that uses the Cauchy-Gauss algorithm to reduce the number of integrations by 1 in each dimension, then a numerical quadrature to solve the resulting equation. This algorithm is more efficient than the discrete approximation, but less versatile since the Cauchy-Gauss algorithm may only be used if the domains are identical. /Journel and Huijbregts, 1978/ provide the FORTRAN implementation of the Cauchy-Gauss, subroutine F, but as provided, subroutine F only solves equation A-3 (i.e., not separated by lag h). This study extends subroutine F to also compute equation A-4 and then to compute the regularised variogram (equation A-2). The coding and extension are verified using MathCAD and the analytical solutions of /Journel and Huijbregts, 1978/.

The resulting variograms are fitted with a model variogram used for input to HYDRASTAR. The functional form of a regularised variogram is most similar to that of a Gaussian model, which is not an admissible type for HYDRASTAR. However, any lag spacing less than the grid spacing is effectively ignored, and thus we fit an exponential model to the regularised variogram for lags greater than the grid spacing of 25 m. This is the model presented in Section 3 of this report.